A New Approach to Three-Dimensional Free-Surface Flow Modeling

Jan J. Leendertse

RAND

The research described in this report was sponsored by The Netherlands Rijkswaterstaat under Contract No. DIV-78 and by The RAND Corporation as part of its program of public service.

ISBN: 0-8330-0947-8

The RAND Publication Series: The Report is the principal publication documenting and transmitting RAND's major research findings and final research results. The RAND Note reports other outputs of sponsored research for general distribution. Publications of The RAND Corporation do not necessarily reflect the opinions or policies of the sponsors of RAND research.

Published by The RAND Corporation
1700 Main Street, P.O. Box 2138, Santa Monica, CA 90406-2138

R-3712-NETH/RC

A New Approach to Three-Dimensional Free-Surface Flow Modeling

Jan J. Leendertse

March 1989

Prepared for
The Netherlands Rijkswaterstaat

RAND

PREFACE

This report relates the development of a three-dimensional model that simulates the hydrodynamics of estuaries and coastal seas. The research was sponsored by The Netherlands Rijkswaterstaat and preparation of this publication was sponsored in part by The RAND Corporation.

Model development began with improvements to an existing three-dimensional model algorithm.[1] In close cooperation with engineers of the Tidal Water Division of The Rijkswaterstaat, we made model experiments of areas near the Dutch coast. These and other earlier experiments indicated that the computation method put very high demands on computer resources, so we modified the existing algorithm to reduce the computation effort an order of magnitude. Although the stability aspects after the modification remained essentially the same as in the earlier model, it appeared that the large timesteps in combination with a turbulence closure model tended to make the model applications unstable. This problem could have been overcome by use of filters, but there was no physical justification of such use.

During these developments, considerable insight was obtained into the behavior of small disturbances in a flow field which led to the completely new formulation of the model described in this report.

---

[1]Jan J. Leendertse, Richard C. Alexander, and Shiao-Kung Liu, *A Three-Dimensional Model for Estuaries and Coastal Seas: Volume I, Principle of Computation*, The RAND Corporation, R-1417-OWRR, December 1973; Shiao-Kung Liu, and Jan J. Leendertse, *A Three-Dimensional Model for Estuaries and Coastal Seas: Volume VI, Bristol Bay Simulations*, The RAND Corporation, R-2405-NOAA, September 1979.

SUMMARY

This report describes an efficient model for the computation of three-dimensional free-surface flows. For the time integration, two different approximations are used in succession. The advection term approximations depend on the flow direction and introduce stability into the computation. The gradients of the advection terms are generally computed directly, whereas the coefficients of the nonlinear terms need to be computed by iteration. Experiments show that only two iterations are required. The finite difference approximations used in the computation are of the second order, and no time filtering or introduction of viscosity is required for stability. The timestep is limited by the accuracy desired in the results. In the formulation, it is assumed that the pressures are hydrostatic. A stability analysis which uses linearized coefficients in the nonlinear terms indicates that the computation method is *unconditionally stable.*

The transport equation used to compute dissolved substances in the fluid also contains approximations for the advection terms which are flow-direction-dependent. The timestep for the transport equation is also limited by the accuracy desired in the results.

To investigate the effect of different timesteps on model results, several experiments were made. These experiments confirmed the analysis of the behavior of the computation method showing that the growth of disturbances with small wavelength and periods is inhibited. With a model of a lake (IJsselmeer), it was shown that with very limited computer resources, effective three-dimensional flow and transport computations can be made.

ACKNOWLEDGMENTS

The author is most indebted to Netherlands Rijkswaterstaat colleague ir. J. Dijkzeul for his exhaustive review of the manuscript and his verification of the agreement between the equations in the report and those in the algorithm. His assistance in finding and correcting errors in the program during the development is appreciated.

The author wants to thank dr. ir. G. S. Stelling of the Delft Hydraulics Laboratory for the many discussions on stability aspects of three-dimensional models and for sharing some of his experience on the use of higher-order asymmetrical finite differences which he first introduced in numerical hydrodynamic computations.

The report was also reviewed by RAND colleagues Dr. M. L. Juncosa and Dr. Shiao-Kung Liu. I would like to thank them for their efforts.

CONTENTS

PREFACE iii

SUMMARY v

ACKNOWLEDGMENTS vii

FIGURES xi

Section

I. INTRODUCTION 1

II. THE APPROXIMATION OF THE ADVECTION TERMS 3

III. FINITE DIFFERENCE EQUATIONS FOR THE INTERIOR FIELD 9

IV. STABILITY ASPECTS OF THE FINITE DIFFERENCE APPROXIMATIONS . 13

V. SEQUENCE OF THE OPERATIONS 18

VI. TRANSPORT EQUATIONS 23

VII. BOUNDARY CONDITIONS 28

VIII. EXPERIMENTS 33

IX. DISCUSSION 48

X. CONCLUSIONS 50

REFERENCES 51

FIGURES

2.1. Grid with computation cell 4
2.2. Approximation of transport by averaging 4
2.3. Approximations for the transport at the location of u_m 5
3.1. Location of variables 10
7.1. Point near boundary 29
7.2. Gridpoints used in the approximation of the cross-advection term 29
7.3. Boundary conditions for the cross-advection term 30
7.4. Transports at a distance Δx from the lower boundary 32
8.1. Basin used for the experiments. The length of the basin is 3400 m, the depth is 7 m. In the figure, the horizontal scale is different from the vertical scale. The horizontal gridsize is 200 m and the vertical scale is 1 m 33
8.2. Computed horizontal velocities in the middle of the basin. Top graph shows velocities with the explicit model (a), the other graphs show the velocities for the new RAND model with a timestep of 6.25 sec (b), 12.5 sec (c), 25 sec (d), 50 sec (e), and 100 sec (f) 34
8.3. Computed vertical velocities near the middle of the basin with a timestep of 6.25 sec (a), 12.5 sec (b), 25 sec (c), 50 sec (d), and 100 sec (e) 36
8.4. Computed concentrations and velocities 24 hours after start of computation at 0.5 m depth (a), 2.5 m depth (b), and 4.5 m depth (c) 37
8.5. Computed concentrations and velocities 48 hours after start of computation at 0.5 m depth (a), 2.5 m depth (b), and 4.5 m depth (c) 38
8.6. Computed concentrations and velocities 72 hours after start of computation at 0.5 m depth (a), 2.5 m depth (b), and 4.5 m depth (c) 39
8.7. Computed concentrations and velocities 96 hours after start of computation at 0.5 m depth (a), 2.5 m depth (b), and 4.5 m depth (c) 40
8.8. Computed time series of the concentration at station A at 0.5 m depth (a), 1.5 m depth (b), 2.5 m depth (c), 3.5 m depth (d), and 4.5 m depth (e) (Δt = 7.5 min) . . . 41
8.9. Computed time series of the concentration at station B at 0.5 m depth (a), 1.5 m depth (b), 2.5 m depth (c), 3.5 m depth (d), and 4.5 m depth (e) (Δt = 7.5 min) . . . 42
8.10. Time series of the concentration at station A at different depth computed with a timestep of 5 min (a), 12 min (b), and 15 min (c) 43
8.11. Time series of the concentration at station B computed with vertical mass and momentum exchange coefficients valued at 0.1 m^2/sec at 0.5 m depth (a), 1.5 m depth (b), 2.5 m depth (c), 3.5 m depth (d), and 4.5 m depth (e) (Δt = 7.5 min) . . . 45
8.12. Time series of the computed concentration at station C (a), D (b), E (c), and F (d) at different depth 46
8.13. Time series of the computed concentration at station G (a), H (b), I (c), and J (d) at different depth 47

I. INTRODUCTION

About fifteen years ago, the first three-dimensional model for free-surface flow computations was developed by the present author and his colleagues at RAND [1–5]. That model in its more developed form used a partly implicit and partly explicit solution scheme. The variables in the vertical direction were computed implicitly for stability reasons. The approach has been quite successful, but the method requires extensive computation when the horizontal gridsizes are small, because the maximum timestep is directly related to the horizontal gridsize by the Courant condition.

In the literature, several attempts to reduce the computational effort have been reported. Blumberg and Mellor [6,7] used the same finite difference equations for the momentum, continuity, and transport equations for temperature and salt as in the RAND model. However, to reduce the computational effort, a so-called mode-splitting technique was introduced by which the advection and the transport of dissolved substances are computed with larger timesteps than for the computation of the free surface. The introduction of this procedure degrades the accuracy of the computation, and in describing an application of this model, Lie-Yauw Oey et al. [8] remark correctly that the model is first-order accurate. Sheng [9,10] uses mode splitting also, but in a more primitive manner than Blumberg and Mellor. This model is also of first-order accuracy.

The applications of Blumberg and Mellor using mode splitting is a logical extension of our earlier formulation, but because this approach degrades accuracy, we have preferred to concentrate our efforts on simultaneous computation of *both* modes in a manner similar to that now used very successfully with two-dimensional models. From the very many applications with two-dimensional models based upon an alternating direction implicit (ADI) computation method on a rectangular grid, it is clear that horizontal flow distributions can be modeled very well, and large-scale eddies can be simulated quite accurately. Consequently, it was advisable to retain these properties in the three-dimensional model. If the advection can be centered properly over the whole timestep, then the computation should be stable. However, the timestep is then limited by the maximum velocity in the field. It appears, also, that such a method is then neutrally stable and very sensitive to all disturbances generated, for example, by the continuously changing dispersion coefficients for the momentum.

While studying the finite difference approximations for the advection terms in the momentum equations in the context of an alternating direction method, it became apparent that a very efficient computational method could be obtained by use of unsymmetrical higher-order approximations for the advection terms. With this computational method, the three-dimensional problem is solved by successive solution of sets of equations that are described in vertical planes. Thus, the three-dimensional problem is broken down to the solution of sets of two-dimensional equations, which in turn can be reduced to the solution of sets of one-dimensional equations.

The finite difference equations for the three-dimensional model based upon this principle are complicated. Also, the order of progress of the computation through the fields of variables is important for a successful simulation. To outline the procedures for this new approach, we will present first the finite difference equations for the advection and then the finite difference equations for the center of the field. We will work directly with finite differences, because these are the equations that are solved numerically on a computer, and also, these are the

equations that were used to formulate, conceptually, the physical processes of the fluid flow. This departs from the usual presentation of models, wherein the problem is defined first with partial-differential equations and subsequently finite difference equations are derived. This classical approach is very difficult and has not been very successful in the construction of two-dimensional models. To a large extent, such an approach was dictated out of necessity when analytical methods were almost the only way that complicated problems could be solved. When computers became available, they were used to assist in solving the complicated formulations originating from a computerless society. At present, in the computer age, we have to make models formulated so that sequential or parallel computation can be used. Moreover, these models have to be adaptive, so that they can be modified when some of the processes, which were originally described by simple relationships, become more complex.

In this report, the stability aspects of the simplified hydrodynamics equations will be presented, after which we will describe the sequence of the operations in one timestep of a simulation. Furthermore, we will show some results of simulations and discuss these results.

II. THE APPROXIMATION OF THE ADVECTION TERMS

The finite difference approximations of the advection terms in the momentum equations and in the transport equation of solute substances appear to be crucial for a successful model. The advection terms in the momentum equations are nonlinear and transfer energy from waves with low frequency to waves with higher frequency. In a finite difference model, such energy transfer should be simulated properly, but the very short waves should ultimately be removed from the simulation. The shortest waves that can be represented have a wavelength of twice the gridsize. Without removal of these very short waves, their amplitudes would grow and the computation would become unstable.

They can be removed by filters, but unfortunately the most commonly used filters also remove waves and disturbances of interest to us and which are a vital part of the processes we want to simulate. In the model presented here, advection term approximations are used that inhibit the generation of these very short waves. The approximations are chosen in such a manner that only the very short waves are influenced, but not the waves in which we are interested. This will be shown clearly with some numerical experiments in Sec. VIII.

Very closely related to the stability problem generated by the finite difference approximations of advection terms in the momentum equations are the approximations of the advection terms in the transport equation for dissolved substances. Here, again, we need to use stable approximations. In addition, it is desirable to have limited dispersion; thus the Fourier components of the concentration field should move practically independent of the frequency. If, indeed, that is the case, a steep front in the concentration field would retain its shape. If there are significant differences in the propagation speed of these components, then the steep front becomes distorted and short-period waves will appear near the front in the simulated concentration field.

In the design of the approximations for the advection terms with the gradients in horizontal direction, we aimed at approximations that were stable and had a minimum accuracy of the second order. Furthermore, approximations were desired that had limited dispersion and that could be expressed directly in available values of the variables. The approximations also had to fit in an alternating direction computation of the water levels. In addition, the advection terms in the transport equations for dissolved substances should naturally be conservative.

To explain the computation procedures that are being used in the algorithm, the advection transport equation will be discussed first. In the most simple conservative form we can write:

$$\frac{\partial P}{\partial t} + \frac{\partial (uP)}{\partial x} = 0 \qquad (2.1)$$

With the commonly used staggered grid systems, the concentration P is defined on the grid at the locations where the pressures are known. The velocities are defined at places between these locations (Fig. 2.1). As a result of this choice, we need to express the transport uP at the designated locations of the velocity when we are considering the mass balance in the cell represented by the shaded are in the figure. In most models, this is accomplished by taking the average of the two adjacent values of the concentration on the grid as shown in Fig. 2.2. This

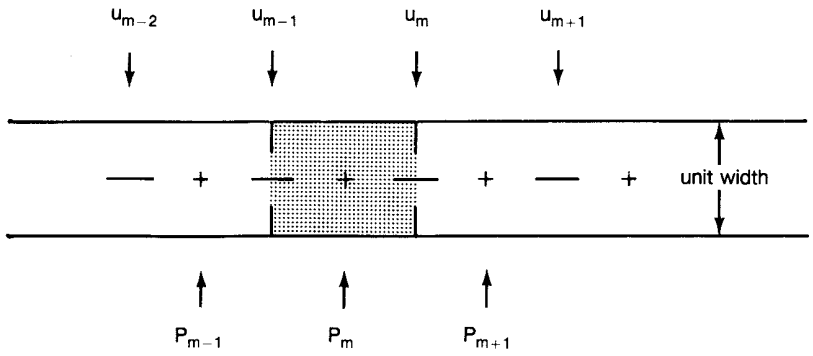

Fig. 2.1—Grid with computation cell

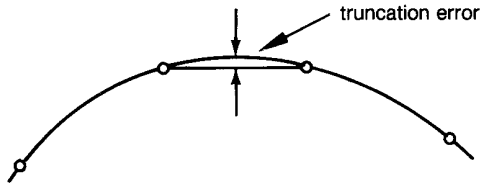

Fig. 2.2—Approximation of transport by averaging

average is an approximation that becomes a "spatial" filter when applied at each point. Rather than averaging the adjacent values of the concentration, we use, alternatively, a weighted average of four values and an extrapolation of two values as shown in Fig. 2.3. Thus, for the transport ($T = uP$) in the cross-section at the location u_m we use, alternatively:

$$T_m = u_m \frac{1}{12} (P_{m-1} + 5P_m + 5P_{m+1} + P_{m+2}) \tag{2.2}$$

and

$$T''_m = u_m \frac{1}{2} (3P_m - P_{m-1}) \tag{2.3}$$

The significance of the superscript ($''$) will be explained below. With the expressions for the transports by Eqs. (2.2) and (2.3), the advection term in Eq. (2.1) is approximated alternatively by:

$$\frac{\partial(uP)}{\partial x} \cong (T_m - T_{m-1})/\Delta x \tag{2.4}$$

and

$$\frac{\partial(uP)}{\partial x} \cong (T''_m - T''_{m-1})/\Delta x \tag{2.5}$$

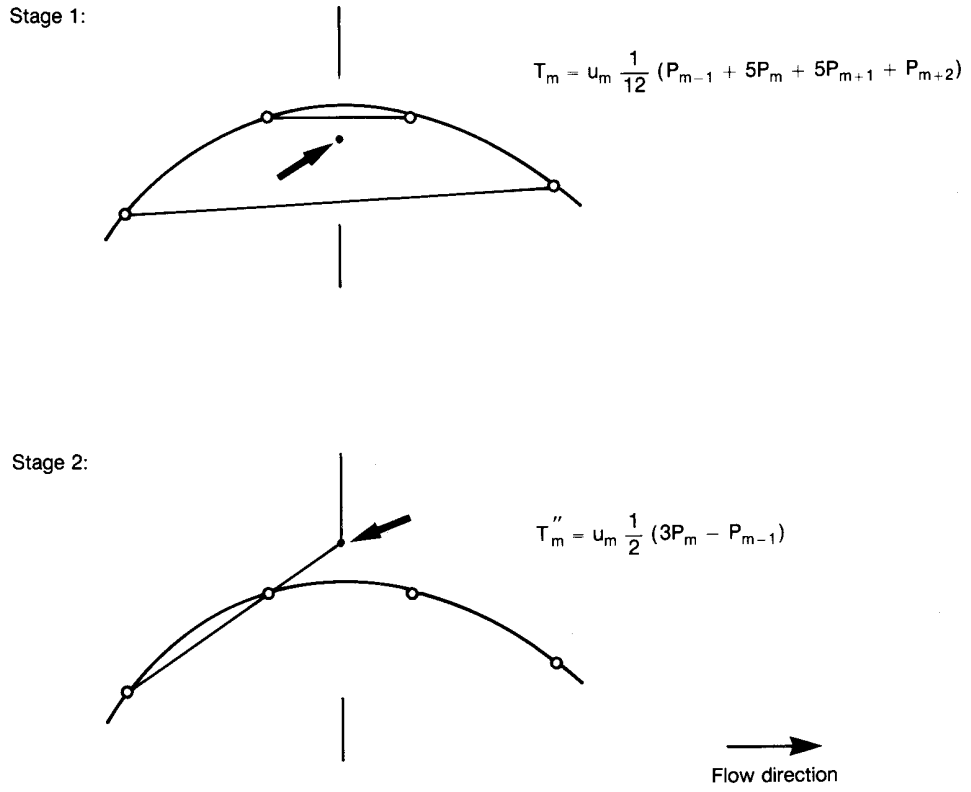

Fig. 2.3—Approximations for the transport at the location of u_m

The truncation errors of the finite difference approximations can be found by Taylor series expansions of the terms in Eqs. (2.2) and (2.3) and by inserting these into the finite difference approximations. We find, then, after omitting terms of the fourth order and higher,

$$(T_m - T_{m-1})/\Delta x =$$
$$u\frac{\partial P}{\partial x} + P\frac{\partial u}{\partial x} + \frac{1}{3}l^2\, u\frac{\partial^3 P}{\partial x^3} + \frac{1}{8}l^2\,\frac{\partial^2 u}{\partial x^2}\,\frac{\partial P}{\partial x} + \frac{5}{12}l^2\,\frac{\partial u}{\partial x}\,\frac{\partial^2 P}{\partial x^2} + \frac{1}{24}l^2\,\frac{\partial^2 u_P}{\partial x^3} + 0(l^4) \qquad (2.6)$$

and

$$(T''_m - T''_{m-1})/\Delta x =$$
$$u\frac{\partial P}{\partial x} + P\frac{\partial u}{\partial x} - \frac{1}{3}l^2\, u\frac{\partial^3 P}{\partial x^3} + \frac{1}{8}l^2\,\frac{\partial^2 u}{\partial x^2}\,\frac{\partial P}{\partial x} - \frac{1}{4}l^2\,\frac{\partial u}{\partial x}\,\frac{\partial^2 P}{\partial x^2} + \frac{1}{24}l^2\,\frac{\partial^3 u_P}{\partial x^3} + 0(l^3) \qquad (2.7)$$

where $l = \Delta x$ is the spatial step size.

For the time-integration of Eq. (2.1), the two advection approximations are used alternatively, the first one with all variables expressed at the lower time level followed by the second approximation with all variables taken at the higher time level. In the time integration, the forward time stepping is with a half-time-step τ. The variables at the time t are indicated without any superscript. The variables at time $t + \tau$ are indicated with a single prime ($'$) as superscript, and the variables at time $t + 2\tau$ are indicated with a double prime ($''$) as a superscript. The two operations can be written as:

$$(P'_m - P_m)/\tau + (T_m - T_{m-1})/\Delta x = 0 \qquad (2.8)$$

and

$$(P''_m - P'_m)/\tau + (T''_m - T''_{m-1})/\Delta x = 0 \qquad (2.9)$$

where we express

$$T''_m = u''_m\,\frac{1}{2}\,(3P''_m - P''_{m-1}) \qquad (2.10)$$

The truncation error for the two-step integration can be determined by first inserting Eq. (2.8) into Eq. (2.9) to eliminate P′ and subsequently making a Taylor series expansion in time using the expressions in Eqs. (2.6) and (2.7). This results in:

$$(P''_m - P_m)/2\tau + (T_m + T''_m - T_{m-1} - T''_{m-1})/2\Delta x = \frac{\partial P}{\partial t} + \frac{\partial (uP)}{\partial x}$$
$$+ \frac{1}{6}\tau^2\,\frac{\partial^3 P}{\partial t^3} + \frac{1}{8}l^2\,\frac{\partial^2 u}{\partial x^2}\,\frac{\partial P}{\partial x} + \frac{1}{12}l^2\,\frac{\partial u}{\partial x}\,\frac{\partial^2 P}{\partial x^2} + \frac{1}{24}l^2\,\frac{\partial^3 u_P}{\partial x^3} + 0(\tau^4, l^3) \qquad (2.11)$$

Thus, the alternate use of Eq. (2.8) and Eq. (2.9) results in a computation method with a second-order accuracy. Note that the truncation does not contain third-order derivatives of P in space.

Up to this point, the discussion about the advection term approximation did concern the advection equation in conservative form. As we plan to use also approximations of the advection terms in nonconservative form, we will now analyze the following equation:

$$\frac{\partial P}{\partial t} + u \frac{\partial P}{\partial x} = 0 \tag{2.12}$$

and if the same principles for the approximation are applied, then we can define

$$T_m = u \frac{1}{12} (P_{m-1} + 5P_m + 5P_{m+1} + P_{m+2}) \tag{2.13}$$

$$T''_m = u \frac{1}{2} (3P''_m - P''_{m-1}) \tag{2.14}$$

and the two-step finite difference approximations of Eq. (2.12) are then again Eqs. (2.8) and (2.9).

The truncation error can be found again with Taylor expansions in a similar manner as established for Eq. (2.11) and results in:

$$(P''_m - P_m)/2\tau + (T_m + T''_m - T_{m-1} - T''_{m-1})/2\Delta x = \frac{\partial P}{\partial t} + u\frac{\partial P}{\partial x} + \frac{1}{6}\tau^2 \frac{\partial^3 P}{\partial t^3} + \frac{u}{2} l\tau^2 \frac{\partial^3 P}{\partial t^2 \partial x} + 0(\tau l^2, \tau^4, l^4) \tag{2.15}$$

Thus the alternate use of Eqs. (2.8) and (2.9) results in a finite difference approximation with a second-order accuracy in time. If the timestep τ is proportional to the gridsize ($\Delta x = l$), then the alternate use of these equations results in a finite difference scheme with third-order accuracy in the spatial dimension.

Rather than expressing the nonconservative transport equation with T_m and T''_m, we can also insert Eq. (2.13) into Eq. (2.8) and Eq. (2.14) into Eq. (2.9) and find the following finite difference equations:

$$(P'_m - P_m)/\tau + u(P_{m+2} + 4P_{m+1} - 4P_{m-1} - P_{m-2})/12\Delta x = 0 \tag{2.16}$$

and

$$(P''_m - P'_m)/\tau + u(3P''_m - 4P''_{m-1} + P''_{m-2})/2\Delta x = 0 \tag{2.17}$$

Stelling [11] investigated the properties of this approximation of the advection equation and found that the approximation was unconditionally stable if the asymmetrical expression in the second step was taken "upstream." Furthermore, phase errors in the solution are small except for the short waves, but their amplitudes are reduced during the integration. He called this approximation the reduced phase error split scheme and used this type of approximation for the cross advection terms of the momentum equations in the finite difference approximation of the vertically integrated hydrodynamic equations. In the three-dimensional model described in this report, this type of approximation will be used for all the advection terms in the horizontal direction in the momentum equations. In the transport equations for the concentration of solutes in the three-dimensional model, the two-step conservative approximation will be used.

III. FINITE DIFFERENCE EQUATIONS FOR THE INTERIOR FIELD

The equations that will be represented are for an interior point of the grid in a simplified form. We will omit the effects of bottom stress and the horizontal momentum exchange. Furthermore, we will simplify the continuity equation and consider only one layer of the finite difference system. Thus, the finite difference equations will represent the following set of partial differential equations:

$$\frac{\partial u}{\partial t} + u\frac{\partial u}{\partial x} + v\frac{\partial v}{\partial y} + w\frac{\partial u}{\partial z} + \nu\frac{\partial^2 u}{\partial z^2} + g\frac{\partial \zeta}{\partial x} = 0 \tag{3.1}$$

$$\frac{\partial v}{\partial t} + u\frac{\partial v}{\partial x} + v\frac{\partial v}{\partial y} + w\frac{\partial v}{\partial z} + \nu\frac{\partial^2 v}{\partial z^2} + g\frac{\partial \zeta}{\partial y} = 0 \tag{3.2}$$

$$\frac{\partial \zeta}{\partial t} + \frac{\partial (hu)}{\partial x} + \frac{\partial (hv)}{\partial y} = 0 \tag{3.3}$$

where

u,v,w = velocity in X,Y, and Z direction, respectively.

ζ = distance between the free surface and a reference level.

g = acceleration due to gravity.

ν = vertical momentum diffusion coefficient.

For the finite difference representation, a staggered grid system is used with the velocities u and v located between the pressure points. The location of the variables on the grid is shown in Fig. 3.1. The half-time-step is again designated by τ. The variables without superscripts are at time t. The variables with a single prime as superscript are at time $t + \tau$, and the variables with a double prime are at time $t + 2\tau$. Subscripts of variables, like ox, +x, 1x, and oxx, which will be explained later, indicate that spatial finite difference approximations of these variables are used. In the explanations of these finite difference approximations, the subscripts n,m,k indicate locations on the three-dimensional grid. We use the Y,X,Z sequence, to conform to the sequence of indexing in computational algorithms.

In the description of the advection terms, we sometimes replace u,v,w by U,V,W, respectively. The introduction of this representation (u = U, etc.) will facilitate the stability analysis that is presented in Sec. IV. The notations to describe the finite difference equations are:

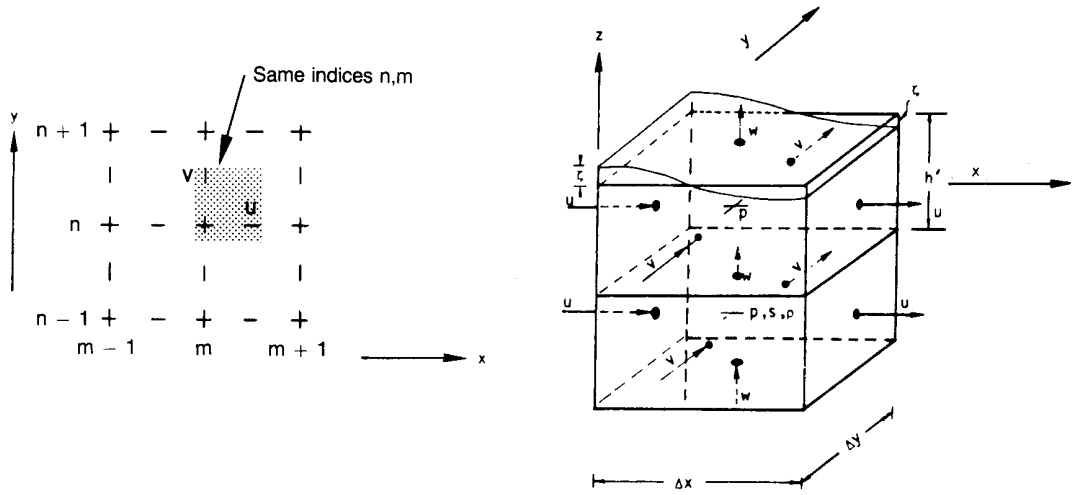

Space-staggered computation grid and relative position of variables

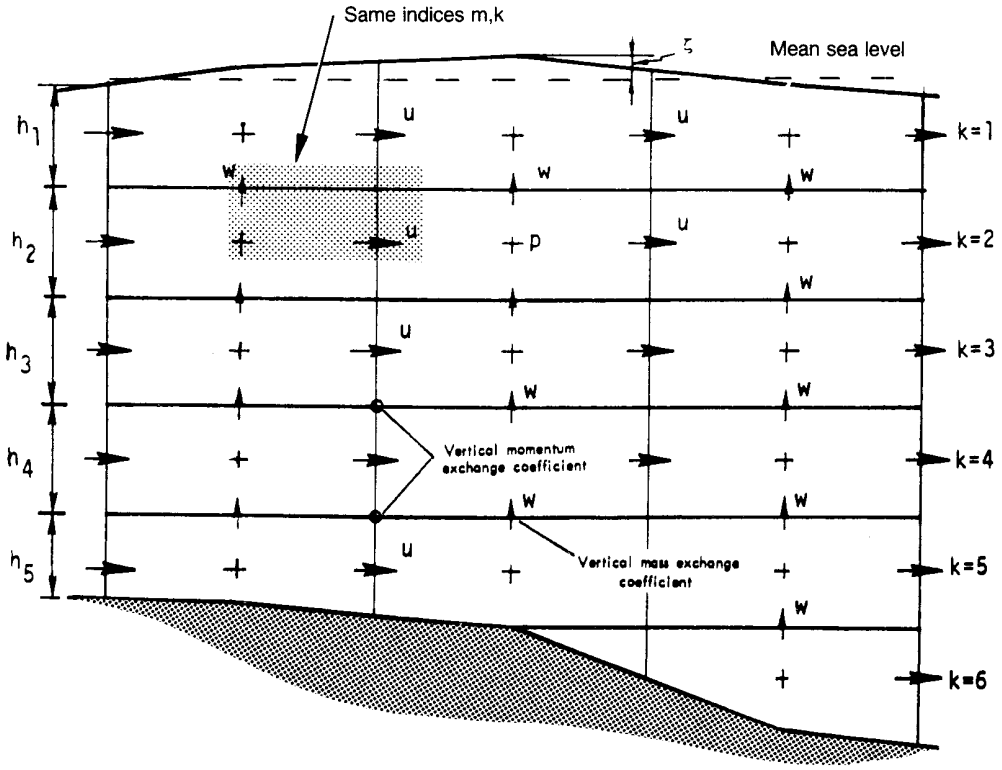

Location of variables on the X-Z plane

Fig. 3.1—Location of variables

$$\zeta_{ox} = (\zeta_{n,m+1} - \zeta_{n,m})/\Delta x \tag{3.4}$$

$$\zeta_{oy} = (\zeta_{n+1,m} - \zeta_{n,m})/\Delta x \tag{3.5}$$

$$\overline{\overline{u_{oz}}}^{z} = (u_{n,m,k+1} - u_{n,m,k})/2\Delta z + (u_{n,m,k} - u_{n,m,k-1})/2\Delta z \tag{3.6}$$

$$\overline{\overline{v'_{oz}}}^{z} = (v'_{n,m,k+1} - v'_{n,m,k})/2\Delta z + (v'_{n,m,k} - v'_{n,m,k-1})/2\Delta z \tag{3.7}$$

$$u_{ozz} = (u_{n,m,k+1} - 2u_{n,m,k} + u_{n,m,k-1})/(\Delta z)^2 \tag{3.8}$$

$$v'_{ozz} = (v'_{n,m,k+1} - 2v'_{n,m,k} + v'_{n,m,k-1})/(\Delta z)^2 \tag{3.9}$$

$$S_{1x}(U',u) =$$

$$U'_{n,m,k}(u_{n,m+2,k} + 4u_{n,m+1,k} - 4u_{n,m-1,k} - u_{n,m-2,k})/12\Delta x \tag{3.10}$$

$$S_{1y}(V'',v') =$$

$$V''_{n,m,k}(v'_{n+2,m,k} + 4v'_{n+1,m,k} - 4v'_{n-1,m,k} - v'_{n-2,m,k})/12\Delta x \tag{3.11}$$

$$S_{1y}(V',u) = (V'_{n,m,k} + V'_{n,m+1,k} + V'_{n-1,m,k} + V'_{n-1,m+1,k}) \times (u_{n+2,m,k} + 4u_{n+1,m,k} - 4u_{n-1,m,k} - u_{n-2,m,k})/48\Delta y \tag{3.12}$$

$$S_{1x}(U'',v') = (U''_{n,m,k} + U''_{n+1,m,k} + U''_{n,m-1,k} + U''_{n+1,m-1,k}) \times (v'_{n,m+2,k} + 4v'_{n,m+1,k} - 4v'_{n,m-1,k} - v'_{n,m-2,k})/48\Delta x \tag{3.13}$$

for $U'_{n,m,k} > 0$

$$S_{+x}(U',u'') = U'_{n,m,k}(3u''_{n,m,k} - 4u''_{n,m-1,k} + u''_{n,m-2,k})/2\Delta x \tag{3.14}$$

for $U'_{n,m,k} \leq 0$

$$S_{+x}(U',u'') = U'_{n,m,k}(-3u''_{n,m,k} + 4u''_{n,m+1,k} - u''_{n,m+2,k})/2\Delta x \tag{3.15}$$

for $V_{n,m,k} > 0$

$$S_{+y}(V,v') = V_{n,m,k}(3v'_{n,m,k} - 4v'_{n-1,m,k} + v'_{n-2,m,k})/2\Delta y \tag{3.16}$$

for $V_{n,m,k} \leq 0$

$$S_{+y}(V,v') = V_{n,m,k}(-3v'_{n,m,k} + 4v'_{n+1,m,k} - v'_{n+2,m,k})/2\Delta y \tag{3.17}$$

for $(U_{n,m,k} + U_{n+1,m,k} + U_{n,m-1,k} + U_{n+1,m-1,k}) > 0$

$$S_{+x}(U,v') = (U_{n,m,k} + U_{n+1,m,k} + U_{n,m-1,k} + U_{n+1,m-1,k}) \times (3v'_{n,m,k} - 4v'_{n,m-1,k} + v'_{n,m-2,k})/8\Delta x \tag{3.18}$$

for $(U_{n,m,k} + U_{n+1,m,k} + U_{n,m-1,k} + U_{n+1,m-1,k}) \leq 0$

$$S_{+x}(U,v') = (U_{n,m,k} + U_{n+1,m,k} + U_{n,m-1,k} + U_{n+1,m-1,k}) \times (-3v'_{n,m,k} + 4v'_{n,m+1,k} - v'_{n,m+2,k})/8\Delta x \tag{3.19}$$

for $(V'_{n,m,k} + V'_{n,m+1,k} + V'_{n-1,m,k} + V'_{n-1,m+1,k}) > 0$

$$S_{+y}(V',u'') = (V'_{n,m,k} + V'_{n,m+1,k} + V'_{n-1,m,k} + V'_{n-1,m+1,k}) \times (3u''_{n,m,k} - 4u''_{n-1,m,k} + u''_{n-2,m,k})/8\Delta x \tag{3.20}$$

$$\text{for } (V'_{n,m,k} + V'_{n,m+1,k} + V'_{n-1,m,k} + V'_{n-1,m+1,k}) \le 0$$

$$S_{+y}(V',u'') = (V'_{n,m,k} + V'_{n,m+1,k} + V'_{n-1,m,k} + V'_{n-1,m+1,k}) \times (-3u''_{n,m,k} + 4u''_{n+1,m,k} - u''_{n+2,m,k})/8\Delta x \tag{3.21}$$

With these notations the basic equations are:

Stage 1:

$$(u' - u)/\tau + S_{1x}(U',u) + S_{1y}(V',u) + W'\overline{u}^{z}_{oz} - \nu u_{ozz} + g\zeta'_{ox} = 0 \tag{3.22}$$

$$(v' - v)/\tau + S_{+x}(U,v') + S_{+y}(V,v') + W\overline{v'}^{z}_{oz} - \nu v'_{ozz} + g\zeta_{oy} = 0 \tag{3.23}$$

$$(\zeta' - \zeta)/\tau + (hu')_{ox} + (hv)_{oy} = 0 \tag{3.24}$$

Stage 2:

$$(u'' - u')/\tau + S_{+x}(U',u'') + S_{+y}(V',u'') + W'\overline{u''}^{z}_{oz} - \nu u''_{ozz} + g\zeta'_{ox} = 0 \tag{3.25}$$

$$(v'' - v')/\tau + S_{1x}(U'',v') + S_{1y}(V'',v') + W''\overline{v'}^{z}_{oz} - \nu v'_{ozz} + g\zeta''_{oy} = 0 \tag{3.26}$$

$$(\zeta'' - \zeta')/\tau + (hu')_{ox} + (hv'')_{oy} = 0 \tag{3.27}$$

Disregarding for the moment the coefficients U, V, and W in the advection terms, then note that in Eq. (3.22) three variables on time level $t + \tau$ appear, namely, the velocity u' and the adjacent two water levels ζ'. In Eq. (3.24) three variables at time $t + \tau$ are also present, namely, ζ' and the two adjacent velocities u'. This is similar to the occurrence of variables in a two-dimensional alternating-direction implicit model.

In Eq. (3.23) the v' variables are present in all three advection terms, as well as in the vertical momentum exchange term, and the inertia term.

In stage 2, v'' and ζ'' are present in Eqs. (3.26) and (3.27). In Eq. (3.25) u'' is present in all three advection terms, in the vertical momentum exchange term, and in the inertia term.

In Eqs. (3.23) and (3.25) the advection terms with gradients in X and Y direction are expressed with variables at the higher time level by "upstream" operators like those shown in Eqs. (3.14) and (3.15). In Eqs. (3.22) and (3.26) the gradients in the advection terms are taken at the lower time level by a centered expression like that in Eq. (3.10). The expressions for the advection terms introduce stability into the computation as will be shown below.

IV. STABILITY ASPECTS OF THE FINITE DIFFERENCE APPROXIMATIONS

Equations (3.22) through (3.27) represent a linear system in the variables u,v,ζ. For the stability analysis, we want to consider the uniform boundedness of the family of amplification matrices going from time t to time t + 2τ. For this analysis which follows methods described by Richtmyer and Morton [12], we consider general solutions of the following type:

$$u(x,y,z,t) = \bar{u}\ \exp[i(\sigma_1 x + \sigma_2 y + \sigma_3 z + \omega t)] \tag{4.1}$$

and similarly for v and ζ:

$$v(x,y,z,t) = \bar{v}\ \exp[i(\sigma_1 x + \sigma_2 y + \sigma_3 z + \omega t)] \tag{4.2}$$

$$\zeta(x,y,z,t) = \bar{\zeta}\ \exp[i(\sigma_1 x + \sigma_2 y + \sigma_3 z + \omega t)] \tag{4.3}$$

Inserting Eqs. (4.1) through (4.3) into Eqs. (3.1) through (3.6) results in the following matrix equations:

$$[A]\ [U'']\ =\ [B]\ [U'] \tag{4.4}$$

$$[C]\ [U']\ =\ [D]\ [U] \tag{4.5}$$

where

$$U = \begin{bmatrix} u \\ v \\ \zeta \end{bmatrix} \tag{4.6}$$

$$A = \begin{bmatrix} a' & 0 & 0 \\ 0 & a'' & \tau g\, \hat{D}_{oy} \\ 0 & \tau h\, \hat{D}_{oy} & 1 \end{bmatrix} \tag{4.7}$$

$$B = \begin{bmatrix} b' & 0 & -\tau g\, \hat{D}_{ox} \\ 0 & b'' & 0 \\ -\tau h\, \hat{D}_{ox} & 0 & 1 \end{bmatrix} \tag{4.8}$$

$$C = \begin{bmatrix} c' & 0 & \tau g\, \hat{D}_{ox} \\ 0 & c'' & 0 \\ \tau h\, \hat{D}_{ox} & 0 & 1 \end{bmatrix} \tag{4.9}$$

$$D = \begin{bmatrix} d' & 0 & 0 \\ 0 & d'' & -\tau g\,\hat{D}_{oy} \\ 0 & -\tau h\,\hat{D}_{oy} & 1 \end{bmatrix} \tag{4.10}$$

and

$$\hat{D}_{ox} = i\,\sin(\sigma_1\Delta x/2)/(\Delta x/2) \tag{4.11}$$

$$\hat{D}_{oy} = i\,\sin(\sigma_2\Delta y/2)/(\Delta y/2) \tag{4.12}$$

$$\hat{D}_{1z} = i\,\sin(\sigma_3\Delta z)/(\Delta z) \tag{4.13}$$

$$a' = 1 + \tau U'\hat{S}_{+x} + \tau V'\hat{S}_{+y} + \tau W'\hat{D}_{1z} + \tau\nu\gamma \tag{4.14}$$

$$a'' = 1 \tag{4.15}$$

$$b' = 1 \tag{4.16}$$

$$b'' = 1 - \tau U''\hat{S}_{1x} - \tau V''\hat{S}_{1y} - \tau W''\hat{D}_{1z} - \tau\nu\gamma \tag{4.17}$$

$$c' = 1 \tag{4.18}$$

$$c'' = 1 + \tau U\,\hat{S}_{+x} + \tau V\,S_{+y} + \tau W\,\hat{D}_{1z} + \tau\nu\gamma \tag{4.19}$$

$$d' = 1 - \tau U'\hat{S}_{1x} - \tau V'\hat{S}_{1y} - \tau W'\hat{D}_{1z} - \tau\nu\gamma \tag{4.20}$$

$$d'' = 1 \tag{4.21}$$

$$\hat{S}_{+x} = \left[[1 - \cos(\sigma_1\Delta x)]^2 + i[2 - \cos(\sigma_1\Delta x)]\,\sin(\sigma_1\Delta x)\right]/\Delta x \tag{4.22}$$

$$\hat{S}_{1x} = i[2 + \cos(\sigma_1\Delta x)]\,\sin(\sigma_1\Delta x)/3\Delta x \tag{4.23}$$

$$\hat{S}_{+y} = \left[[1 - \cos(\sigma_2\Delta y)]^2 + i[2 - \cos(\sigma_2\Delta y)]\,\sin(\sigma_2\Delta y)\right]/\Delta y \tag{4.24}$$

$$\hat{S}_{1y} = i[2 + \cos(\sigma_2\Delta y)]\,\sin(\sigma_2\Delta y)/3\Delta y \tag{4.25}$$

$$\gamma = 2[1 - \cos(\sigma_3\Delta z)]/(\Delta z)^2 \tag{4.26}$$

The amplification matrix can now be derived from Eqs. (4.4) and (4.5)

$$G = A^{-1}BC^{-1}D \tag{4.27}$$

Stability is insured if the family of matrices is uniformly bounded. Following the analysis by Stelling [11], this can be verified by introducing a matrix L to symmetrize A, B, C, and D by similarity transformation. The matrix L is defined by

$$L = \begin{bmatrix} 1 & 0 & 0 \\ 0 & 1 & 0 \\ 0 & 0 & \sqrt{h/g} \end{bmatrix} \tag{4.28}$$

The amplification matrix can then be written:

$$G = LL^{-1}A^{-1}LL^{-1}BLL^{-1}C^{-1}LL^{-1}DLL^{-1} \tag{4.29}$$

or

$$G = L(L^{-1}AL)^{-1}(L^{-1}BL)(L^{-1}CL)^{-1}(L^{-1}DL)L^{-1} \tag{4.30}$$

Finally we can write for the amplification matrix:

$$G = L\,A'^{-1}B'C'^{-1}D'L^{-1} \tag{4.31}$$

where

$$A' = \begin{bmatrix} a' & 0 & 0 \\ 0 & 1 & \tau\sqrt{gh}\hat{D}_{oy} \\ 0 & \tau\sqrt{gh}\hat{D}_{oy} & 1 \end{bmatrix} \tag{4.32}$$

$$B' = \begin{bmatrix} 1 & 0 & -\tau\sqrt{gh}\hat{D}_{ox} \\ 0 & b'' & 0 \\ -\tau\sqrt{gh}\hat{D}_{ox} & 0 & 1 \end{bmatrix} \tag{4.33}$$

$$C' = \begin{bmatrix} 1 & 0 & \tau\sqrt{gh}\hat{D}_{ox} \\ 0 & c'' & 0 \\ \tau\sqrt{gh}\hat{D}_{ox} & 0 & 1 \end{bmatrix} \tag{4.34}$$

$$D' = \begin{bmatrix} d' & 0 & 0 \\ 0 & 1 & -\tau\sqrt{gh}\hat{D}_{oy} \\ 0 & -\tau\sqrt{gh}\hat{D}_{oy} & 1 \end{bmatrix} \tag{4.35}$$

Equation (4.31) implies the following relation:

$$\| G^k \| \leq \|L\,A'^{-1}\|\,\|B'\,C'^{-1}\|^k\,\|D'A'^{-1}\|^{k-1}\,\|D'L^{-1}\| \tag{4.36}$$

for any positive integer k. Thus, for stability of Eqs. (3.1) to (3.6) it is sufficient that

$$\|B'\,C'^{-1}\| \leq 1 \tag{4.37}$$

and

$$\| D'A'^{-1} \| \leq 1 \tag{4.38}$$

The matrices A′ and D′ may also be written as

$$A' = \begin{bmatrix} a' & 0 \\ 0 & A_s' \end{bmatrix} \tag{4.39}$$

$$D' = \begin{bmatrix} d' & 0 \\ 0 & D_s' \end{bmatrix} \tag{4.40}$$

where

$$A_s' = \begin{bmatrix} 1 & \tau\sqrt{gh}\hat{D}_{oy} \\ \tau\sqrt{gh}\hat{D}_{oy} & 1 \end{bmatrix} \tag{4.41}$$

$$D_s' = \begin{bmatrix} 1 & -\tau\sqrt{gh}\hat{D}_{oy} \\ -\tau\sqrt{gh}\hat{D}_{oy} & 1 \end{bmatrix} \tag{4.42}$$

Note that D_s' is adjoint to A_s' by the fact that the respective elements are the complex conjugates. Thus we may write:

$$D'A'^{-1} = \begin{bmatrix} d'/a' & 0 \\ 0 & A_s'^{H} A_s'^{-1} \end{bmatrix} \tag{4.43}$$

For the proof of (4.38) we need the following lemma [11]:

Lemma 4.1:

If A is a nonsingular matrix, then $A^H A^{-1}$ is a unitary matrix.

By use of this lemma it follows that

$$\| D'A'^{-1} \| \leq \text{Max} \ (|d'/a'|, 1) \tag{4.44}$$

From Eqs. (4.14) and (4.20) it is found that $|d'/a'| \leq 1$, thus also:

$$\| D'A'^{-1} \| \leq 1 \tag{4.45}$$

Similarly, it can be found:

$$\| B'C'^{-1} \| \leq 1 \tag{4.46}$$

Thus, the finite difference approximations represented by Eqs. (3.22) to (3.27) are stable.

From the absolute values of the ratios of $|d'/a'|$ and $|b'/c'|$, it can be noted that the stability is influenced by several factors. The vertical momentum exchange stabilizes the computation according to the exchange coefficient. Also, the real part of the upstream operators in a' and c' contributes to the stability according to the current intensity. Even when one of these operators is not taken upstream, but downstream, for which the sign changes, then the computation will still be stable as long as the other current component is larger than the one taken downstream.

If the advection is expressed upstream, and the coefficients of the nonlinear terms are constant during the timestep, the computation is *unconditionally* stable.

V. SEQUENCE OF THE OPERATIONS

In describing the sequence of the computation, we will omit the detailed description of the boundary conditions, because this would distract the reader from the subject at hand. The boundary conditions will be described in detail.

The solutions of the finite difference equations for each stage are solved iteratively ($p = 1, \ldots P$). In general, iterations are required only for the expressions for the advection term coefficients and for the upstream gradients in the advection terms in case the local flow direction is different from the dominant flow direction. The iteration level of the v velocities in such cases is indicated by a superscript (*); thus, when the velocity has just been computed during the ongoing iteration, the iteration level is p, otherwise the iteration level is $p - 1$.

In the first half-time-step (stage 1) of the multistep operation, the horizontal velocities in the vertical planes in the Y direction are computed first. The computation of these velocities is implicit in the vertical. For the interior of the field, the following momentum equation, which now contains, also, the horizontal diffusion terms and the coriolis term ($f\bar{u}$), can be written:

$$(v^p - v)/\tau + S_{+x}(u,v^*) + S_{+y}(v,v^*) + \overline{\bar{w}^y v^p}^z_{oz} + f\bar{u} - \nu v^p_{zz} - D(v^{p-1}_{xx} + v^{p-1}_{yy}) + g\zeta_{oy} = 0 \qquad (5.1)$$

where

$$\text{for } (u_{n,m,k} + u_{n+1,m,k} + u_{n,m-1,k} + u_{n+1,m-1,k}) > 0$$

$$S_{+x}(u,v^*) = (u_{n,m,k} + u_{n+1,m,k} + u_{n,m-1,k} + u_{n+1,m-1,k}) \times (3v^p_{n,m,k} - 4v^*_{n,m-1,k} + v^*_{n,m-2,k})/8\Delta x \qquad (5.2)$$

$$\text{for } (u_{n,m,k} + u_{n+1,m,k} + u_{n,m-1,k} + u_{n+1,m-1,k}) \leq 0$$

$$S_{+x}(u,v') = (u_{n,m,k} + u_{n+1,m,k} + u_{n,m-1,k} + u_{n+1,m-1,k}) \times (-3v^p_{n,m,k} + 4v^*_{n,m+1,k} - v^*_{n,m+2,k})/8\Delta x \qquad (5.3)$$

$$\text{for } v_{n,m,k} > 0$$

$$S_{+y}(v,v^*) = v_{n,m,k}\ (3v^p_{n,m,k} - 4v^*_{n-1,m,k} + v^*_{n-2,m,k})/2\Delta y \qquad (5.4)$$

$$\text{for } v_{n,m,k} \leq 0$$

$$S_{+y}(v,v^*) = v_{n,m,k}\ (-3v^p_{n,m,k} + 4v^*_{n+1,m,k} - v^*_{n+2,m,k})/2\Delta y \qquad (5.5)$$

$$v_{xx}^{p-1} = (v_{n,m-1,k}^{p-1} - 2v_{n,m,k}^{p-1} + v_{n,m+1,k}^{p-1})/(\Delta x)^2 \tag{5.6}$$

$$v_{yy}^{p-1} = (v_{n+1,m,k}^{p-1} - 2v_{n,m,k}^{p-1} + v_{n-1,m,k}^{p-1})/(\Delta y)^2 \tag{5.7}$$

$$v_{zz}^{p} = (v_{n,m,k+1}^{p} - 2v_{n,m,k}^{p} + v_{n,m,k-1}^{p})/(\Delta z)^2 \tag{5.8}$$

$$\bar{\bar{u}} = (u_{n,m,k} + u_{n+1,m,k} + u_{n,m-1,k} + u_{n+1,m-1,k})/4 \tag{5.9}$$

The sets of equations for a number of points in the vertical can be solved very rapidly as each momentum equation (Eq. 5.1) contains three variables in that vertical.

In each vertical plane in the Y direction, the systems of equations are solved initially in the Y direction. The sequence of computations of these planes starts in the X direction. If the signs of the u and v flow are all positive, then the whole field is solved in one iteration (except for the horizontal diffusion terms), because all variables with superscript (*) are directly available for computation. As flow reversals are nearly always present in the computation field, two iterations are generally required. The second iteration is performed in opposite order. In the second iteration, the upstream variables in the advection terms, which were in the previous iteration on the lower time level, are now on the latest time level.

For the solution of the set of equations in each vertical, the set for each point at n, m can be written after multiplication by the layer thickness:

$$a_k v_{n,m,k-1}^{p} + b_k v_{n,m,k}^{p} + c_k v_{n,m,k+1}^{p} = d_k^{p-1} \tag{5.10}$$

where

$$a_k = \tau\left[-2\nu + \frac{1}{2} h_k (w_{n,m,k} + w_{n+1,m,k})\right]/(h_k + h_{k-1}) \tag{5.11}$$

$$c_k = \tau\left[-2\nu - \frac{1}{2} h_k (w_{n,m,k+1} + w_{n+1,m,k+1})\right]/(h_k + h_{k+1}) \tag{5.12}$$

$$\begin{aligned} b_k = h_k\Big[& 1 + \frac{3\tau}{2\Delta x} \mid v_{n,m,k}\mid \\ & + \frac{3\tau}{8\Delta y} \mid (u_{n,m,k} + u_{n+1,m,k} + u_{n,m-1,k} + u_{n+1,m-1,k})\mid\Big] - a_k - c_k \end{aligned} \tag{5.13}$$

$$\begin{aligned} d_k^{p-1} = h_k \Big[& v_{n,m,k} + \tau \mid (u_{n,m,k} + u_{n+1,m,k} + u_{n,m-1,k} + u_{n+1,m-1,k})\mid \times \\ & (4v_{n,m\pm1,k}^{*} - v_{n,m\pm2,k}^{*})/8\Delta x \\ & + \tau|v_{n,m,k}|\ (4v_{n\pm1,m,k}^{*} - v_{n\pm2,m,k}^{*})/2\Delta y - \frac{\tau}{\Delta x} g(\zeta_{n+1,m} - \zeta_{n,m}) \\ & - \tau f(u_{n,m,k} + u_{n+1,m,k} + u_{n,m-1,k} + u_{n+1,m-1,k})/4 \\ & + \tau D(v_{n,m+1,k}^{p-1} - 2v_{n,m,k}^{p-1} + v_{n,m-1,k}^{p-1})/(\Delta x)^2 \\ & + \tau D(v_{n+1,m,k}^{p-1} - 2v_{n,m,k}^{p-1} + v_{n-1,m,k}^{p-1})/(\Delta y)^2\Big] \end{aligned} \tag{5.14}$$

To solve the sets of equations (5.10) for a column of points going from k = 1 to k = K, a double sweep method is used. For the boundary condition we have:

at the surface (k = 1) $\qquad a_k = 0$

for the bottompoint (k = K) $\qquad c_K = 0$

For the surface and bottom layers, stress terms have to be added to the equations, these will be discussed below.

The solutions of the other equations in stage 1 are even more complicated, because Eq. (3.22) and Eq. (3.24) are coupled vertically in u as well as through the water-level gradient term in the momentum equation, and the water level in the continuity equation. Here again some iterations are required. For the u momentum equation in the middle of the field and in the central layers (k = 2, . . . K − 1), we have in stage 1:

$$(u^q - u)/\tau + S_{1x}(u^{q-1},u) + S_{1y}(v',u) + \overline{\overline{w^{q-1}}^{x}}^{z} u_{oz} - (\nu u_{oz})_{oz} - f\bar{\bar{v}}' - D(u_{xx} + u_{yy}) + g\zeta^q_{ox} = 0 \qquad (5.15)$$

where

$$S_{1x}(u^{q-1},u) = u^{q-1}_{n,m,k} \times (u_{n,m+2,k} + 4u_{n,m+1,k} - 4u_{n,m-1,k} - u_{n,m-2,k})/12\Delta x \qquad (5.16)$$

$$S_{1y}(v',u) = (v'_{n,m,k} + v'_{n,m+1,k} + v'_{n-1,m,k} + v'_{n-1,m+1,k}) \times (u_{n+2,m,k} + 4u_{n+1,m,k} - 4u_{n-1,m,k} - u_{n-2,m,k})/48\Delta y \qquad (5.17)$$

or in a more compact form

$$(u^q_k - u_k)/\tau + g\zeta^q_{ox} + F^{q-1}_k = 0 \qquad (5.18)$$

with

$$F^{q-1}_k = S_{1x}(u^{q-1},u) + S_{1y}(\bar{\bar{v}}',u) + \overline{\overline{w^{q-1}}^{x}}^{z} u_{oz} - f\bar{\bar{v}}' - (\nu u_{oz})_{oz} - D(u_{xx} + u_{yy}) \qquad (5.19)$$

To compute all the water levels iteratively (p = 1, 2) in a row n, the momentum equations are integrated over the vertical in every point of that row, and we obtain the following vertically integrated momentum equation:

$$(U' - U^{p-1})/\tau + \sum_{k=2}^{K} h_k F^{q-1}_k + (h_1 + \overline{\zeta^{p-1}}^{x}) F^{q-1}_1 + g\left(\sum_{k=1}^{K} h_k + \overline{\zeta^{p-1}}^{x}\right) \zeta^p_{ox} = 0 \qquad (5.20)$$

where

$$U^{p-1} = (h_1 + \overline{\zeta^{p-1}}^{x})u_1 + \sum_{k=2}^{K} h_k u_k \qquad (5.21)$$

The momentum equation (5.20) can also be written as:

$$(U' - U^{p-1})/\tau + R^{p-1} + g\, H^{p-1}\, \zeta^{p}_{ox} = 0 \tag{5.22}$$

where

$$R^{p-1} = \sum_{k=2}^{K} h_k F_k^{q-1} + (h_1 + \overline{\zeta^{p-1}}^{x})\, F_1^{q-1} \tag{5.23}$$

and

$$H^{p-1} = \sum_{k=1}^{K} h_k + \overline{\zeta^{p-1}}^{x} \tag{5.24}$$

The integration over the vertical of the continuity equations results in:

$$(\zeta^{p} - \zeta)/\tau + U'_{ox} + V_{oy} = 0 \tag{5.25}$$

where

$$V = (h_1 + \zeta^{y})\, v_1 + \sum_{k=2}^{K} h_k v_k \tag{5.26}$$

In Eq. (5.25) there are three variables to be computed, namely, the new water level and the values of the momentum (U') at each side of the water-level point. Adjacent to it we find the momentum equations (5.22), which contain also three variables, namely, the momentum U' and two water levels. The variables U and ζ are located on a two-dimensional grid, but as we are considering these variables only on a particular row n, in the discussion of the solution of these variables, we need only to indicate their position by a single subscript. Thus we can write:

$$-\frac{\tau}{\Delta x} g H^{p-1}_{m-1} \zeta^{p}_{m-1} + U'_{m-1} + \frac{\tau}{\Delta x} g H^{p-1}_{m-1} \zeta^{p}_{m} = U^{p-1}_{m-1} - \tau R^{p-1}_{m-1} \tag{5.27}$$

$$-\frac{\tau}{\Delta x} U'_{m-1} + \zeta^{p}_{m} + \frac{\tau}{\Delta x} U'_{m} = \zeta_{m} - \tau V_{oy} \tag{5.28}$$

$$-\frac{\tau}{\Delta x} g H^{p-1}_{m} \zeta^{p}_{m} + U'_{m} + \frac{\tau}{\Delta x} g H^{p-1}_{m} \zeta^{p}_{m+1} = U^{p-1}_{m} - \tau R^{p-1}_{m} \tag{5.29}$$

If we now eliminate U'_{m-1} and U'_{m} we obtain:

$$-\left(\frac{\tau}{\Delta x}\right)^2 g H^{p-1}_{m-1} \zeta^{p}_{m-1} + \left[1 + \left(\frac{\tau}{\Delta x}\right)^2 g (H^{p-1}_{m-1} + H^{p-1}_{m})\right] \zeta^{p}_{m} - \left(\frac{\tau}{\Delta x}\right)^2 g H^{p-1}_{m} \zeta^{p}_{m+1} =$$

$$\frac{\tau}{\Delta x} (U^{p-1}_{m-1} - \tau R^{p-1}_{m-1} - U^{p-1}_{m} + \tau R^{p-1}_{m}) + \zeta_{m} - \tau V_{oy} \tag{5.30}$$

This can be written as:

$$A_m \zeta^p_{m-1} + B_m \zeta^p_m + C_m \zeta^p_{m+1} = D_m \tag{5.31}$$

where

$$A_m = -\left(\frac{\tau}{\Delta x}\right)^2 g H^{p-1}_{m-1} \tag{5.32}$$

$$B_m = \left[1 + \left(\frac{\tau}{\Delta x}\right)^2 g \left(H^{p-1}_{m-1} + H^{p-1}_m\right) \right] \tag{5.33}$$

$$C_m = -\left(\frac{\tau}{\Delta x}\right)^2 g H^{p-1}_m \tag{5.34}$$

$$D_m = \frac{\tau}{\Delta x}\left(U^{p-1}_{m-1} - \tau R^{p-1}_{m-1} - U^{p-1}_m + \tau R^{p-1}_m\right) + \zeta_m - \tau V_{oy} \tag{5.35}$$

The computation of the water levels and the u-velocities in a vertical plane in the X direction starts with the computation of F^{q-1}_k for all the points in the vertical plane, by means of Eq. (5.19) for q = 1. Subsequently, U^{p-1}, R^{p-1}, and H^{p-1} are computed using Eqs. (5.21), (5.23), and (5.24), respectively, to provide data for the solution of the set of equations represented by Eq. (5.31). After the water levels ζ are found for p = 1, the vertically integrated equations are solved again with the just-computed water levels in U, R, and H by which we find ζ for p = 2. With these results, we are now able to find the velocities u by means of Eq. (5.18) for q = 1. After computing the horizontal velocities, the vertical velocities can be computed by means of a continuity equation:

$$(w^q_{m,n,k} - w^q_{m,n,k+1})/h_k + u^q_{ox} + v_{oy} = 0 \tag{5.36}$$

This completes the first iteration (q = 1), and the whole procedure is repeated, again, starting by recomputing F_k for every point in the vertical plane.

In the numerous experiments we have made, it was found that after two iterations (q = 1, 2) sufficient accuracy was obtained, if the computation was started with extrapolated values from previous time levels. To solve the vertically integrated equations, it was sufficient to compute these also twice (p = 1, 2).

The second step of the computation follows the pattern described above for the first step. First, the u″ velocities are computed with the presure gradient at $t + \tau$, then the v″ velocities with the pressure gradient at $t + 2\tau$, implicitly with the continuity equations.

VI. TRANSPORT EQUATIONS

The design of the finite difference approximations for the transport equations followed the pattern of approximation of the hydrodynamic equations. The concentrations were defined at centered locations between the velocity points. As a result, the concentration at the location of the velocities had to be expressed as functions of the concentration values of points in the vicinity of the location of the velocity as described in Sec. II. In previous models [1–5], this concentration was expressed as the average of the concentration at the adjacent concentration points. This approximation is simple and conservative, but experience in its application shows that near steep fronts a disturbance wave is generated, often giving rise to negative concentrations. This phenomenon is generated mainly by the different propagation speeds of the Fourier components of the concentration.

Several investigators have designed more accurate schemes. For example, Leonard [13] computes the concentration at the location of the velocities by a quadratic extrapolation from the values of the concentration "upstream" from the velocity point under consideration. This method was also simple, but the timestep was limited.

In the present model, two approximations are used. One is a simple upstream approximation; the second approximation uses weighted averages from adjacent points. Thus, for the advection transport through a section at the location of u, we use for the first approximation

$$T_{n,m,k} = \frac{1}{12}\,(P_{n,m+2,k} + 5P_{n,m+1,k} + 5P_{n,m,k} + P_{n,m-1,k})u_{n,m,k}\,h^u_{n,m,k} \qquad (6.1)$$

where

$$h^u_{n,m,k} = \text{layer thickness at the location of } u_{n,m,k}$$

For the second approximation, we use if $u_{n,m,k} \geq 0.0$

$$T_{n,m,k} = \frac{1}{2}(3P_{n,m+1,k} - P_{n,m+2,k})u_{n,m,k}\,h^u_{n,m,k} \qquad (6.2)$$

or if $u_{n,m,k} \geq 0.0$

$$T_{n,m,k} = \frac{1}{2}(3P_{n,m,k} - P_{n,m-1,k})u_{n,m,k}\,h^u_{n,m,k} \qquad (6.3)$$

In each of the two expressions for the transport equations, we use upstream differences in one direction and the averages in the other direction. Iterations are used in the computations. The iterations are indicated by the superscript p ($p = 1, \ldots P$). In some instances, an asterisk is used as a superscript. This occurs in the "upstream" approximation of the advection transport term. The asterisk means that a value at iteration level p is used when the value has just been computed and is available. If it is not available on that iteration level, then the iteration level $p - 1$ is used. Thus, for step 1 in the middle of the field, we have the following expression:

$$h_k(P^p_{n,m,k} - P_{n,m,k}) + \frac{\tau}{\Delta x}(T'_{n,m,k} - T'_{n,m-1,k}) + \frac{\tau}{\Delta y}(Q_{n,m,k} - Q_{n-1,m,k}) + \frac{\tau}{2\Delta z}h_k(F_{n,m,k} - F_{n,m,k+1} + F'_{n,m,k} - F'_{n,m,k+1}) = 0 \qquad (6.4)$$

where

$$\text{if } u'_{n,m,k} < 0.0$$
$$T'_{n,m,k} = \left[\frac{1}{2}u'_{n,m,k}(3P^*_{n,m+1,k} - P^*_{n,m+2,k}) - \frac{\kappa}{\Delta x}(P^{p-1}_{n,m+1,k} - P^{p-1}_{n,m,k})\right]h^u_{n,m,k} \qquad (6.5)$$

$$\text{if } u'_{n,m,k} \geq 0.0$$
$$T'_{n,m,k} = \left[\frac{1}{2}u'_{n,m,k}(3P^*_{n,m,k} - P^*_{n,m-1,k}) - \frac{\kappa}{\Delta x}(P^{p-1}_{n,m+1,k} - P^{p-1}_{n,m,k})\right]h^u_{n,m,k} \qquad (6.6)$$

$$\text{if } u'_{n,m-1,k} < 0.0$$
$$T'_{n,m-1,k} = \left[\frac{1}{2}u'_{n,m-1,k}(3P^*_{n,m,k} - P^*_{n,m+1,k}) - \frac{\kappa}{\Delta x}(P^{p-1}_{n,m,k} - P^{p-1}_{n,m-1,k})\right]h^u_{n,m-1,k} \qquad (6.7)$$

$$\text{if } u'_{n,m-1,k} \geq 0.0$$
$$T'_{n,m-1,k} = \left[\frac{1}{2}u'_{n,m-1,k}(3P^*_{n,m-1,k} - P^*_{n,m-2,k}) - \frac{\kappa}{\Delta x}(P^{p-1}_{n,m,k} - P^{p-1}_{n,m-1,k})\right]h^u_{n,m-1,k} \qquad (6.8)$$

and

$$Q_{n,m,k} = \left[\frac{1}{12}(P_{n+2,m,k} + 5P_{n+1,m,k} + 5P_{n,m,k} + P_{n-1,m,k})v_{n,m,k} - \frac{\kappa}{\Delta y}(P_{n+1,m,k} - P_{n,m,k})\right]h^v_{n,m,k} \qquad (6.9)$$

$$Q_{n-1,m,k} = \left[\frac{1}{12}(P_{n+1,m,k} + 5P_{n,m,k} + 5P_{n-1,m,k} + P_{n-2,m,k})v_{n-1,m,k} - \frac{\kappa}{\Delta y}(P_{n,m,k} - P_{n-1,m,k})\right]h^v_{n-1,m,k} \qquad (6.10)$$

Furthermore, if the layer thickness is the same in all layers, then

$$F_{n,m,k} = \frac{1}{2}w'_{n,m,k}(P_{n,m,k-1} + P_{n,m,k}) - \frac{\nu}{\Delta z}(P_{n,m,k-1} - P_{n,m,k}) \qquad (6.11)$$

$$F_{n,m,k+1} = \frac{1}{2}w'_{n,m,k+1}(P_{n,m,k} + P_{n,m,k+1}) - \frac{\nu}{\Delta z}(P_{n,m,k} - P_{n,m,k+1}) \qquad (6.12)$$

$$F'_{n,m,k} = \frac{1}{2}w'_{n,m,k}(P^p_{n,m,k-1} + P^p_{n,m,k}) - \frac{\nu}{\Delta z}(P^p_{n,m,k-1} - P^p_{n,m,k}) \qquad (6.13)$$

$$F'_{n,m,k+1} = \frac{1}{2}w'_{n,m,k+1}(P^p_{n,m,k} + P^p_{n,m,k+1}) - \frac{\nu}{\Delta z}(P^p_{n,m,k} - P^p_{n,m,k+1}) \qquad (6.14)$$

Otherwise

$$F_{n,m,k} = w'_{n,m,k}\left[\frac{h_k}{(h_k + h_{k-1})}P_{n,m,k-1} + \frac{h_{k-1}}{(h_k + h_{k-1})}P_{n,m,k}\right] - \frac{2\nu}{(h_k + h_{k-1})}P_{n,m,k-1} + \frac{2\nu}{(h_k + h_{k-1})}P_{n,m,k} \qquad (6.15)$$

$$F'_{n,m,k} = w'_{n,m,k}\left[\frac{h_k}{(h_k + h_{k-1})}P^p_{n,m,k-1} + \frac{h_{k-1}}{(h_k + h_{k-1})}P^p_{n,m,k}\right] - \frac{2\nu}{(h_k + h_{k-1})}P^p_{n,m,k-1} + \frac{2\nu}{(h_k + h_{k-1})}P^p_{n,m,k} \qquad (6.16)$$

$$F_{n,m,k+1} = w'_{n,m,k+1}\left[\frac{h_k}{(h_k + h_{k+1})}P_{n,m,k+1} + \frac{h_{k+1}}{(h_k + h_{k+1})}P_{n,m,k}\right] + \frac{2\nu}{(h_k + h_{k+1})}P_{n,m,k+1} - \frac{2\nu}{(h_k + h_{k+1})}P_{n,m,k} \qquad (6.17)$$

$$F'_{n,m,k+1} = w'_{n,m,k+1}\left[\frac{h_k}{(h_k + h_{k+1})}P^p_{n,m,k+1} + \frac{h_{k+1}}{(h_k + h_{k+1})}P^p_{n,m,k}\right] + \frac{2\nu}{(h_k + h_{k+1})}P^p_{n,m,k+1} - \frac{2\nu}{(h_k + h_{k+1})}P^p_{n,m,k} \qquad (6.18)$$

The transport equation (6.4) can now be written:

$$\left[- \frac{\tau\nu}{(h_{k-1} + h_k)} + \frac{\frac{1}{2}\tau w'_{n,m,k}}{(h_{k-1} + h_k)}\, h_k\right]P^p_{n,m,k-1}$$

$$+ \left[h_k + \frac{\frac{1}{2}\tau w'_{n,m,k}}{(h_{k-1} + h_k)}\, h_{k-1} - \frac{\frac{1}{2}\tau w'_{n,m,k+1}}{(h_k + h_{k+1})}\, h_{k+1} + \frac{\tau\nu}{(h_{k-1} + h_k)} + \frac{\tau\nu}{(h_k + h_{k+1})} + \frac{\tau}{\Delta x}(p_{m,k} - p_{m-1,k})\right]P^p_{n,m,k}$$

$$+ \left[- \frac{\tau\nu}{(h_{k+1} + h_k)} - \frac{\frac{1}{2}\tau w'_{n,m,k+1}}{(h_{k+1} + h_k)}\, h_k\right]P^p_{n,m,k+1} =$$

$$h_k P_{n,m,k} - \frac{\tau}{\Delta y}(Q_{n,m,k} - Q_{n-1,m,k})$$

$$- \frac{\frac{1}{2}\tau w'_{n,m,k}}{(h_{k-1} + h_k)}(h_{n,m,k}P_{n,m,k-1} + h_{n,m,k-1}P_{n,m,k})$$

$$+ \frac{\frac{1}{2}\tau w'_{n,m,k+1}}{(h_k + h_{k+1})}(h_{n,m,k}P_{n,m,k+1} + h_{n,m,k+1}P_{n,m,k})$$

$$+ \frac{\tau\nu}{(h_{k-1} + h_k)}(P_{n,m,k-1} - P_{n,m,k}) - \frac{\tau\nu}{(h_{k+1} + h_k)}(P_{n,m,k} - P_{n,m,k+1})$$

$$+ \frac{\tau}{\Delta x}(- q_{m,k} + q_{m-1,k}) + \frac{\tau}{\Delta x}(r_{m,k} - r_{m-1,k}) \qquad (6.19)$$

where

$$r_{m,k} = [\frac{\kappa}{\Delta x}(P^{p-1}_{n,m+1,k} - P^{p-1}_{n,m,k})]h^u_{n,m,k} \tag{6.20}$$

if $u'_{n,m,k} < 0.0$ and the computation proceeds in negative direction

$$p_{m,k} = 0 \tag{6.21}$$

$$q_{m,k} = \frac{1}{2}u'_{n,m,k}h^u_{n,m,k}(3P^p_{n,m+1,k} - P^p_{n,m+2,k}) \tag{6.22}$$

if $u'_{n,m,k} < 0.0$ and the computation proceeds in positive direction

$$p_{m,k} = 0 \tag{6.23}$$

$$q_{m,k} = \frac{1}{2}u'_{n,m,k}h^u_{n,m,k}(3P^{p-1}_{n,m+1,k} - P^{p-1}_{n,m+2,k}) \tag{6.24}$$

if $u'_{n,m,k} \geq 0.0$ and the computation proceeds in negative direction

$$p_{m,k} = 0 \tag{6.25}$$

$$q_{m,k} = \frac{1}{2}u'_{n,m,k}h^u_{n,m,k}(3P^{p-1}_{n,m,k} - P^{p-1}_{n,m-1,k}) \tag{6.26}$$

if $u'_{n,m,k} \geq 0.0$ and the computation proceeds in positive direction

$$p_{m,k} = \frac{3}{2}u'_{n,m,k}h^u_{n,m,k} \tag{6.27}$$

$$q_{m,k} = -\frac{1}{2}u'_{n,m,k}h^u_{n,m,k}P^p_{n,m-1,k} \tag{6.28}$$

and

$$r_{m-1,k} = \frac{\kappa}{\Delta x}h^u_{n,m-1,k}(P^{p-1}_{n,m,k} - P^{p-1}_{n,m-1,k}) \tag{6.29}$$

if $u'_{n,m-1,k} < 0.0$ and the computation proceeds in negative direction

$$p_{m-1,k} = \frac{3}{2}u'_{n,m-1,k}h^u_{n,m-1,k} \tag{6.30}$$

$$q_{m-1,k} = -\frac{1}{2}u'_{n,m-1,k}h^u_{n,m-1,k}P^p_{n,m+1,k} \tag{6.31}$$

if $u'_{n,m-1,k} < 0.0$ and the computation proceeds in positive direction

$$p_{m-1,k} = 0 \tag{6.32}$$

$$q_{m-1,k} = \frac{1}{2}u'_{n,m-1,k}h^u_{n,m-1,k}(3P^{p-1}_{n,m,k} - P^{p-1}_{n,m+1,k}) \tag{6.33}$$

if $u'_{n,m-1,k} > 0.0$ and the computation proceeds in negative direction

$$p_{m-1,k} = 0.0 \tag{6.34}$$

$$q_{m-1,k} = \frac{1}{2}u'_{n,m-1,k}h^u_{n,m-1,k}(3P^{p-1}_{n,m-1,k} - P^{p-1}_{n,m-2,k}) \tag{6.35}$$

if $u'_{n,m-1,k} > 0.0$ and the computation proceeds in positive direction

$$p_{m-1,k} = 0.0 \tag{6.36}$$

$$q_{m-1,k} = \frac{1}{2}u'_{n,m-1,k}h^u_{n,m-1,k}(3P^p_{n,m-1,k} - P^p_{n,m-2,k}) \tag{6.37}$$

Equation (6.19) can also be written as:

$$A_{m,k}P^{p}_{n,m,k-1} + B_{m,k}P^{p}_{n,m,k} + C_{m,k}P^{p}_{n,m,k+1} = D_{m,k} \tag{6.38}$$

where

$$A_{m,k} = -\frac{\tau\nu}{(h_{k-1} + h_k)} + \frac{\frac{1}{2}\tau w'_{n,m,k}}{(h_{k-1} + h_k)}\, h_k \tag{6.39}$$

$$B_{m,k} = h_k + \frac{\frac{1}{2}\tau w'_{n,m,k}}{(h_{k-1} + h_k)}\, h_{k-1} - \frac{\frac{1}{2}\tau w'_{n,m,k+1}}{(h_k + h_{k+1})}\, h_{k+1} + \frac{\tau\nu}{(h_{k-1} + h_k)} + \frac{\tau\nu}{(h_k + h_{k+1})} + \frac{\tau}{\Delta x}(p_{m,k} - p_{m-1,k}) \tag{6.40}$$

$$C_{m,k} = -\frac{\tau\nu}{(h_{k+1} + h_k)} - \frac{\frac{1}{2}\tau w'_{n,m,k+1}}{(h_{k+1} + h_k)}\, h_k \tag{6.41}$$

$$\begin{aligned} D_{m,k} = {} & h_k P_{n,m,k} - \frac{\tau}{\Delta y}(Q_{n,m,k} - Q_{n-1,m,k}) \\ & - \frac{\frac{1}{2}\tau w'_{n,m,k}}{(h_{k-1} + h_k)}(h_{n,m,k}P_{n,m,k-1} + h_{n,m,k-1}P_{n,m,k}) \\ & + \frac{\frac{1}{2}\tau w'_{n,m,k+1}}{(h_k + h_{k+1})}(h_{n,m,k+1}P_{n,m,k} + h_{n,m,k}P_{n,m,k+1}) \\ & + \frac{\tau\nu}{(h_{k-1} + h_k)}(P_{n,m,k-1} - P_{n,m,k}) - \frac{\tau\nu}{(h_{k+1} + h_k)}(P_{n,m,k} - P_{n,m,k+1}) \\ & + \frac{\tau}{\Delta x}(-q_{m,k} + q_{m-1,k}) + \frac{\tau}{\Delta x}(r_{m,k} - r_{m-1,k}) \end{aligned} \tag{6.42}$$

Equation (6.38) is an equation with three unknown values of concentration, which are all in a vertical column. These sets of equations can be solved rapidly by a double-sweep method. To solve all these sets, we solve all values in a vertical plane in the X direction successively in the positive direction. Then the following iteration is made in the negative direction. In practice, only two iterations are required (p = 1, 2).

For the solution of step 2, the upstream variables are taken in the Y direction, and all variables in the vertical planes in that direction are also computed with two iterations similar to the computation of the first step.

VII. BOUNDARY CONDITIONS

At the surface, wind introduces movements of the water. This is modeled by adding a windstress term to the momentum equations for the top layer. For example, to the right side of Eq. (5.14) is added for k = 1:

$$\tau S_v = \tau\ \theta\ \rho_a W^2 \cos\ \psi\ /\rho \tag{7.1}$$

where

S_v = windstress in Y direction
θ = windstress coefficient
ρ_a = density of air
ρ = density of water
W = windspeed
ψ = angle between wind direction and the positive y direction

At the bottom, a bottomstress term is added to the momentum equations. For example, to the momentum equation in Y direction in the first stage of the equation the following term is added to the right side of Eq. (5.13):

$$\tau S_{by} = \tau g\ [v^2_{n,m,k} + \tfrac{1}{4}(u_{n,m,k} + u_{n,m-1,k} + u_{n+1,m,k} + u_{n-1,m+1,k})^2]^{1/2}\ /(C^2) \tag{7.2}$$

where

S_{by} = bottomstress
g = acceleration of gravity
C = Chezy coefficient

In the finite difference approximations of the momentum equations and the transport equations as described in Secs. III and VI, in each direction a total of five points of a variable are used to compute the variable on the new time level. Thus, near boundaries, other approximations need to be used. As the boundary conditions for the momentum equations of a two-dimensional model were carefully evaluated by Stelling [11], the same approximations were applied for the boundaries of the horizontal layers of the three-dimensional model.

Of the boundary conditions for each term of the advection terms in both stages of the finite difference approximations, one or more conditions will be given as an example. For the advection the gradient in the direction of the flow in the momentum equation in X direction we take for the point near the boundary (Fig. 7.1):

Stage 1:

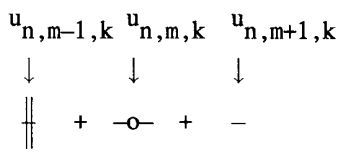

$$u\frac{\partial u}{\partial x} \cong \begin{cases} 0, & \text{if } u'_{n,m,k} \geq 0 \\ u'_{n,m,k}(u_{n,m+1,k} - u_{n,m,k}) & \text{if } u'_{n,m,k} < 0 \end{cases} \tag{7.3}$$

Stage 2:

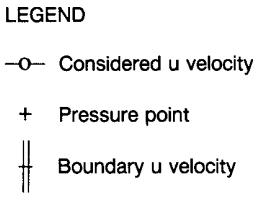

$$u\frac{\partial u}{\partial x} \cong \begin{cases} 0, & \text{if } u'_{n,m,k} \geq 0 \\ u'_{n,m,k}(u'_{n,m+1,k} - u'_{n,m,k}) & \text{if } u'_{n,m,k} < 0 \end{cases} \tag{7.4}$$

Fig. 7.1—Point near boundary

For the approximation of the cross-advection term in the middle of the field, many points are involved as shown in Fig. 7.2. As a result, we had to select among many choices for the approximations near the boundary. Sixteen different conditions can be identified for the availability of points to describe the cross-velocity gradient in relation to the boundaries of the model. These conditions are shown in Fig. 7.3. In the middle of the field away from the boundaries we have condition 1.

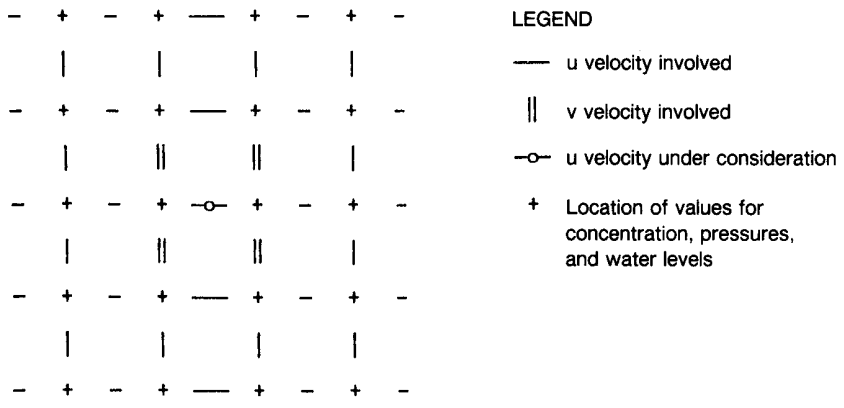

Fig. 7.2—Gridpoints used in the approximation of the cross-advection term

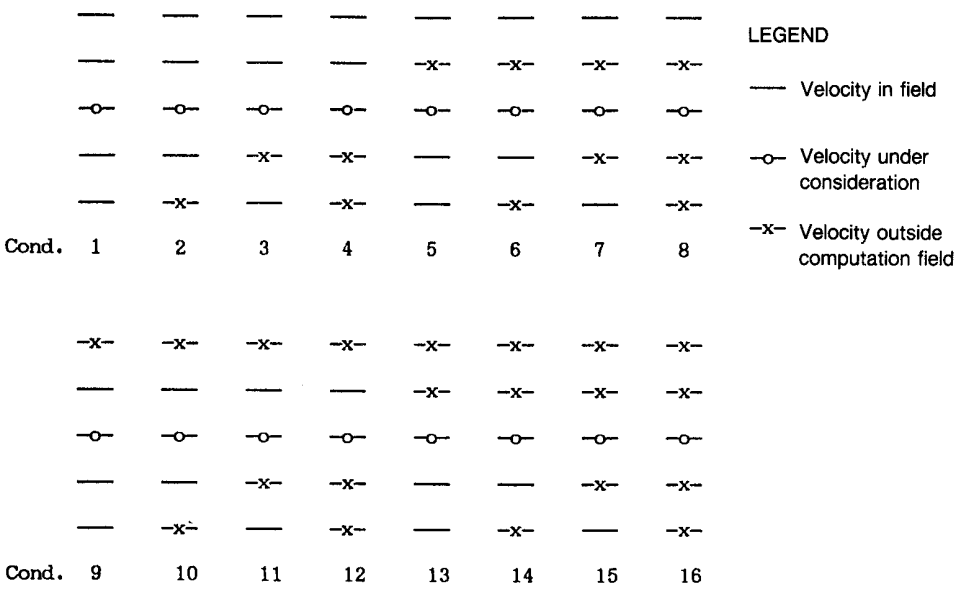

Fig. 7.3—Boundary conditions for the cross-advection term

Several different approximations are used for each of the two stages of the computation.

In stage 1, we use for condition 1, which is the most commonly used approximation for the middle of the field:

$$v\frac{\partial u}{\partial y} \cong (v'_{n,m+1,k} + v'_{n,m,k} + v'_{n-1,m+1,k} + v'_{n-1,m,k}) \times (u_{n+2,m,k} + 4u_{n+1,m,k} - 4u_{n-1,m,k} - u_{n-2,m,k})/(48\Delta y) \quad (7.5)$$

In stage 1, for conditions 2, 9, and 10, we use:

$$v\frac{\partial u}{\partial y} \cong (v'_{n,m+1,k} + v'_{n,m,k} + v'_{n-1,m+1,k} + v'_{n-1,m,k}) \times (u_{n+1,m,k} - u_{n-1,m,k})/(8\Delta y) \quad (7.6)$$

and for all other conditions in stage 1 the cross-advection term is set to zero.

In stage 2, the approximations depend on the current direction and on the sequence of the computation. The iteration level of the velocity values expressing the gradient are taken at iteration level p if the computation progresses in the direction of the flow, and at iteration level p − 1 if the computation progresses opposite the direction of the flow. The involved variables are indicated by the superscript (*).

If $(v'_{n,m+1,k} + v'_{n,m,k} + v'_{n-1,m+1,k} + v'_{n-1,m,k}) > 0$, we use for conditions 1, 5, 9, and 13:

$$v\frac{\partial u}{\partial y} \cong (v'_{n,m+1,k} + v'_{n,m,k} + v'_{n-1,m+1,k} + v'_{n-1,m,k}) \times (3u^*_{n,m,k} - 4u^*_{n-1,m,k} + u^*_{n-2,m,k})/(8\Delta y) \tag{7.7}$$

and for conditions 2, 6, 10, and 14:

$$v\frac{\partial u}{\partial y} \cong (v'_{n,m+1,k} + v'_{n,m,k} + v'_{n-1,m+1,k} + v'_{n-1,m,k}) \times (u'_{n,m,k} - u'_{n-1,m,k})/(4\Delta y) \tag{7.8}$$

and the cross-advection term is set to zero for all other conditions of stage 2.

If $(v'_{n,m-1,k} + v'_{n,m,k} + v'_{n-1,m-1,k} + v'_{n-1,m,k}) \leq 0$, we use for conditions 1, 2, 3, and 4:

$$v\frac{\partial u}{\partial y} \cong (v'_{n,m+1,k} + v'_{n,m,k} + v'_{n-1,m+1,k} + v'_{n-1,m,k}) \times (-3u^*_{n,m,k} + 4u^*_{n+1,m,k} - u^*_{n+2,m,k})/(8\Delta y) \tag{7.9}$$

and for conditions 9, 10, 11, and 12:

$$v\frac{\partial u}{\partial y} \cong (v'_{n,m-1,k} + v'_{n,m,k} + v'_{n-1,m-1,k} + v'_{n-1,m,k}) \times (u'_{n+1,m,k} - u'_{n,m,k})/(4\Delta y) \tag{7.10}$$

and for this cross-current direction, the cross-advection term is set to zero for all other conditions of stage 2.

The boundary conditions for the momentum equation in the Y direction are approximated in a similar manner.

For the transport equations, the approximations that are being used depend on the distance of the cross-section under consideration to the closed boundary. At the closed boundary the transport of solutes is zero. In a cross-section that is a distance Δx from the closed boundary on the western (left) side of the field, we use (Fig. 7.4):

For stage 1:

$$\text{if } u'_{n,m,k} < 0.0$$

$$T'_{n,m,k} = \left[\frac{1}{2}u'_{n,m,k}(3P^*_{n,m+1,k} - P^*_{n,m+2,k}) - \frac{\kappa}{\Delta x}(P^{p-1}_{n,m+1,k} - P^{p-1}_{n,m,k})\right]h^u_{n,m,k} \tag{7.11}$$

$$\text{If } u'_{n,m,k} \geq 0.0$$

$$T'_{n,m,k} = \left[u'_{n,m,k} P^{*}_{n,m,k} - \frac{\kappa}{\Delta x}(P^{p-1}_{n,m+1,k} - P^{p-1}_{n,m,k})\right] h^{u}_{n,m,k} \qquad (7.12)$$

and for stage 2:

$$T''_{n,m,k} = \left[\frac{1}{2}(P'_{n,m,k} + P'_{n,m+1,k})\, u_{n,m,k} - \frac{\kappa}{\Delta x}(P'_{n,m+1,k} - P'_{n,m,k})\right] h^{u}_{n,m,k} \qquad (7.13)$$

The approximations for the transports through cross-sections near other boundaries are similar.

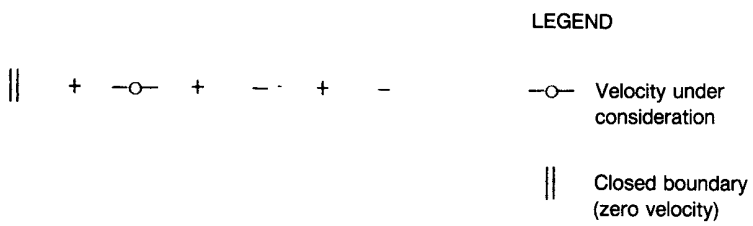

For stage 1:

$$T_{n,m,k} = \left[\frac{1}{2}(P_{n,m,k} + P_{n,m+1,k})\, u_{n,m,k} - \frac{\kappa}{\Delta x}(P_{n,m+1,k} - P_{n,m,k})\right] h^{u}_{n,m,k}$$

for stage 2:

$$\text{if } u''_{n,m,k} < 0.0$$

$$T''_{n,m,k} = \left[\frac{1}{2} u''_{n,m,k}(3P^{*}_{n,m+1,k} - P^{*}_{n,m+2,k}) - \frac{\kappa}{\Delta x}(P^{p-1}_{n,m+1,k} - P^{p-1}_{n,m,k})\right] h^{u}_{n,m,k}$$

$$\text{if } u''_{n,m,k} \geq 0.0$$

$$T''_{n,m,k} = \left[u''_{n,m,k} P^{*}_{n,m,k} - \frac{\kappa}{\Delta x}(P^{p-1}_{n,m+1,k} - P^{p-1}_{n,m,k})\right] h^{u}_{n,m,k}$$

Fig. 7.4—Transports at a distance Δx from the lower boundary

VIII. EXPERIMENTS

The first experiment was to compute an oscillation in a rectangular basin. The length of the basin is 3400 m and the depth is 7 m. The horizontal gridsize was 200 m and the vertical gridsize was 1 m. The experiment began with a sinusoidal disturbance of the water surface with an amplitude of 0.25 m and a wavelength of 6800 m (Fig. 8.1). The experiment was the same as one reported with an earlier explicit three-dimensional model [1].

The computations were made with timesteps of 6.25 sec, 12.5 sec, 25 sec, 50 sec, and 100 sec. The computed velocities were abstracted from the top layer in the middle of the basin. In the model experiment with the explicit model, the velocities were also abstracted in the middle of the basin. The timestep for the explicit model experiment was 5 sec, which was somewhat shorter than the maximum timestep of 8.3 sec allowed for stability reasons.

The computed horizontal velocities for the different experiments are shown in Fig. 8.2. The velocity time series from the experiments with a timestep of 25 sec or shorter shows a gradual growth of higher harmonics. These cannot be observed in the results of the experiments with a timestep of 50 sec and a timestep of 100 sec (Figs. 8.2e and 8.2f). Note that the basic oscillation decays very slowly and that the wave propagation is somewhat slower for the simulation with a timestep of 100 sec.

The vertical velocities of the water surface were also abstracted in the middle of the basin. As this location is near the node of the primary oscillation, only the higher harmonics

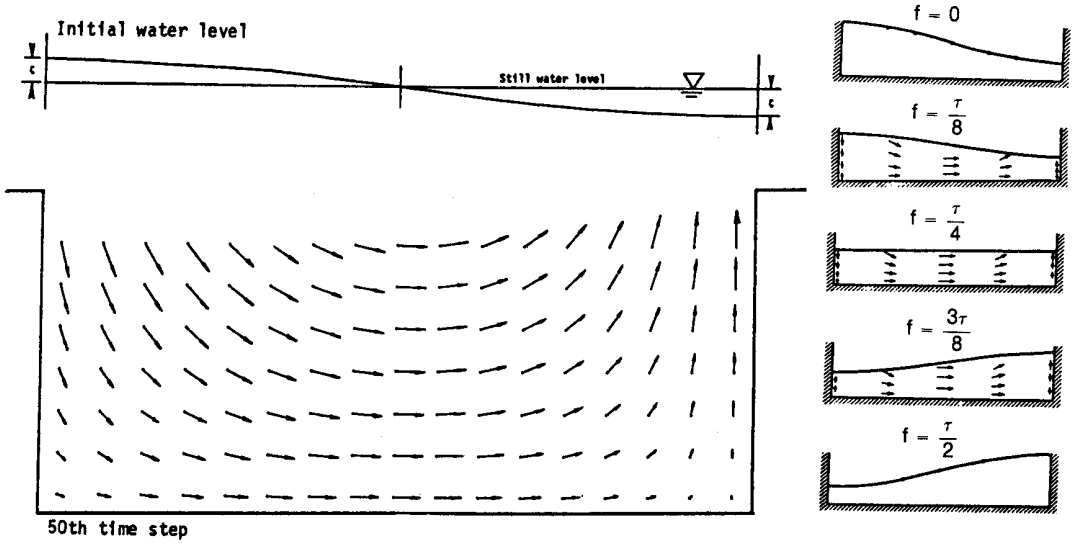

Fig. 8.1—Basin used for the experiments. The length of the basin is 3400 m, the depth is 7 m. In the figure, the horizontal scale is different from the vertical scale. The horizontal gridsize is 200 m and the vertical scale is 1 m.

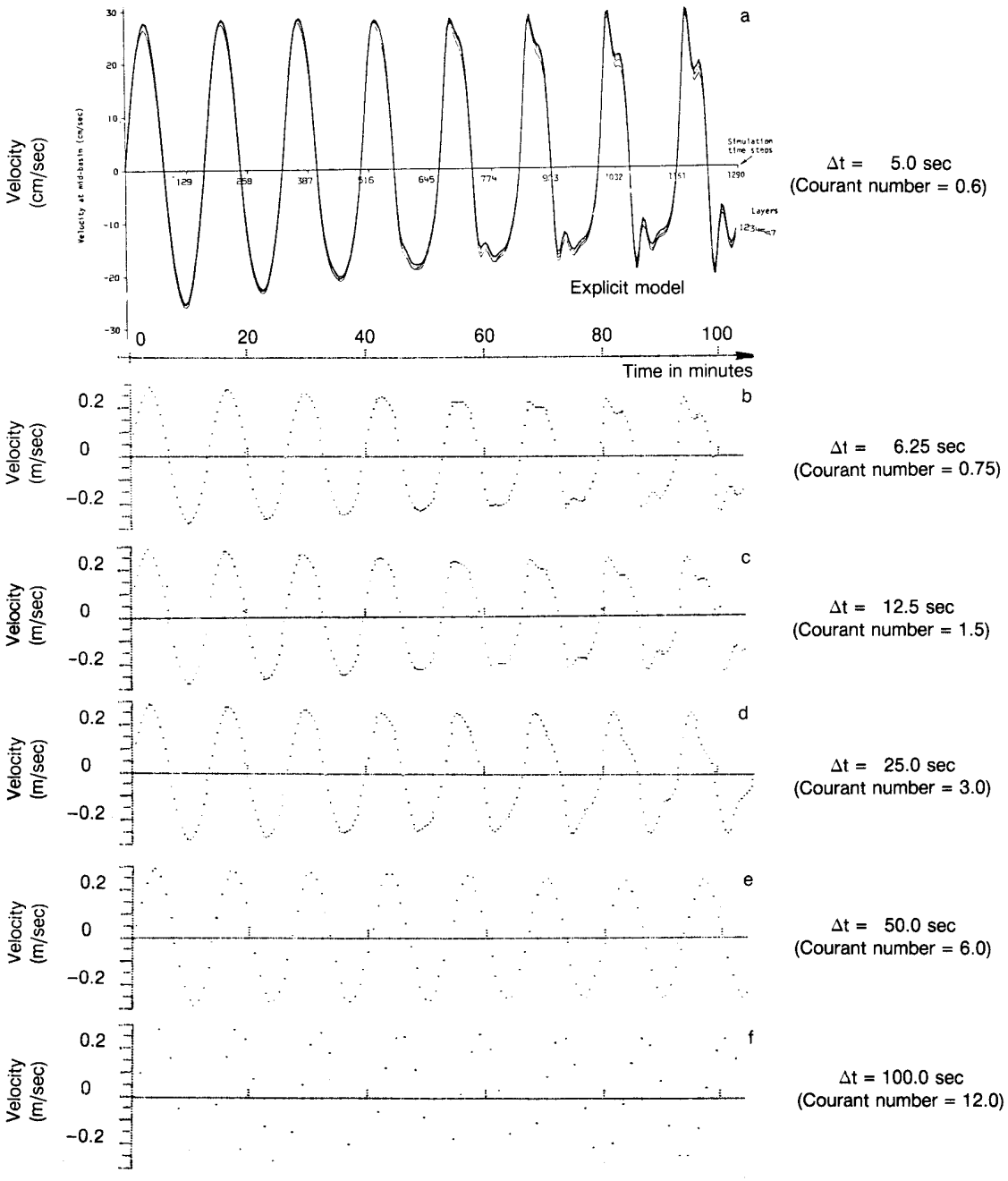

Fig. 8.2—Computed horizontal velocities in the middle of the basin. Top graph shows velocities with the explicit model (a), the other graphs show the velocities for the new RAND model with a timestep of 6.25 sec (b), 12.5 sec (c), 25 sec (d), 50 sec (e), and 100 sec (f)

of the primary oscillation are present in the time series (Fig. 8.3). For the simulation with a timestep of 100 sec, the vertical velocities are very small. In this case the first harmonic is represented by about four points in time.

The two figures give considerable insight into the behavior of the computation method. Note that in the beginning of the simulations, the amplitudes of the first harmonic all grow at about the same rate, but the final amplitudes appear to depend on the resolution in time. Thus, energy transfer from the primary mode to the first harmonic is apparently always present, but the damping of the harmonic thus generated depends on the time representation.

The second series of experiments was made with a model of the IJsselmeer. The IJsselmeer is an artificial lake created in The Netherlands surrounded in part by reclaimed land. A dam at its northwestern extremity separates the lake from the shallow tidal waters behind the Frisian Islands. The dam contains two sets of discharge sluices, only one of which was modeled. The IJssel, which is a branch of the Rhine River, discharges into the lake. The maximum depth of the lake is about 7 meters.

The lake was represented by a grid of 36 $\times$ 21 points in the horizontal plane. The grid-size was 1200 m, the vertical representation was made by five layers of 1 m, and the bottom layer was taken at 1.5 m. We assumed an inflow into the IJssel of 500 m^3/sec, and the discharge of the sluices was set also at 500 m^3/sec.

To represent a spill in the IJssel, we use a concentration of a solute of 50 gr/m^3 in the inflow into the lake from the IJssel. This concentration was maintained for the first hour of the simulation, and also for the second 12 hour period of the first day, after which the concentration dropped gradually during the first 6 hours of the second day to the background level of 1 gr/m^3 in the lake. A wind driven circulation was generated by a southeasterly wind of about 11.3 m/sec. For the vertical exchange coefficients of momentum and mass, a value of 0.00075 m^2/sec was used, and the horizontal momentum and mass exchange coefficient was set at 5 m^2/sec.

A 20 day simulation was made with a timestep of 7.5 min. Figure 8.4 shows the concentration fields at 0.5 m depth, at 2.5 m depth, and at 4.5 m depth at the end of the first day. Also shown are the current velocities at the different depths. At the surface, the water movements are generally in the direction of the wind.

After one day, only a small part of the lake is influenced by the spill, but in the following days the pollutant spreads rapidly in a complicated pattern. Figures 8.5 through 8.7 show the concentration fields at daily intervals. Particularly during the first few days, considerable differences in concentration over the vertical exist in the southern part of the lake. This is shown more clearly in the time series of the concentration in Figs. 8.8 and 8.9.

To investigate the effect of the timestep on the solution of the transport equation, three experiments were made with the same inputs, but with different timesteps. Figure 8.10 shows the computed time series of the concentration at station B for computations with a timestep of 5 min, 12, and 15 min. The computed time series is essentially the same, thus the timestep has very limited influence on the solution.

As three-dimensional models are not readily available to many investigators, the much more common two-dimensional models are sometimes used for management and policy investigations. It is generally well recognized that two-dimensional models underestimate the spread of discharged pollutants under influence of wind, but on the other hand, it is very common to use simple models for management and policy decisions. To obtain some insight into the differences between results of two- and three-dimensional simulations, a simulation was made with the same inputs as the simulations described above, but only the vertical mass and

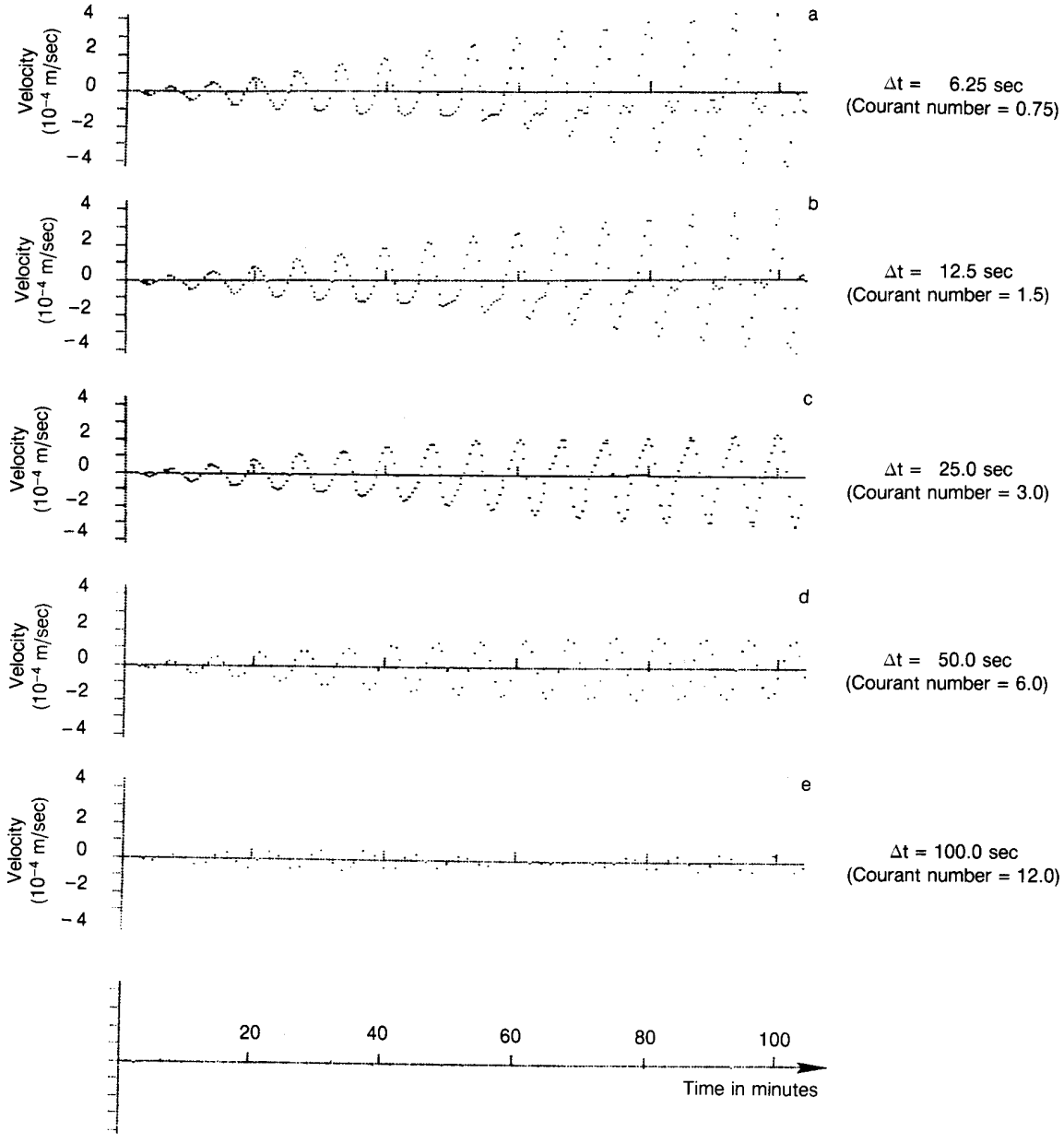

Fig. 8.3—Computed vertical velocities near the middle of the basin with a timestep of 6.25 sec (a), 12.5 sec (b), 25 sec (c), 50 sec (d), and 100 sec (e)

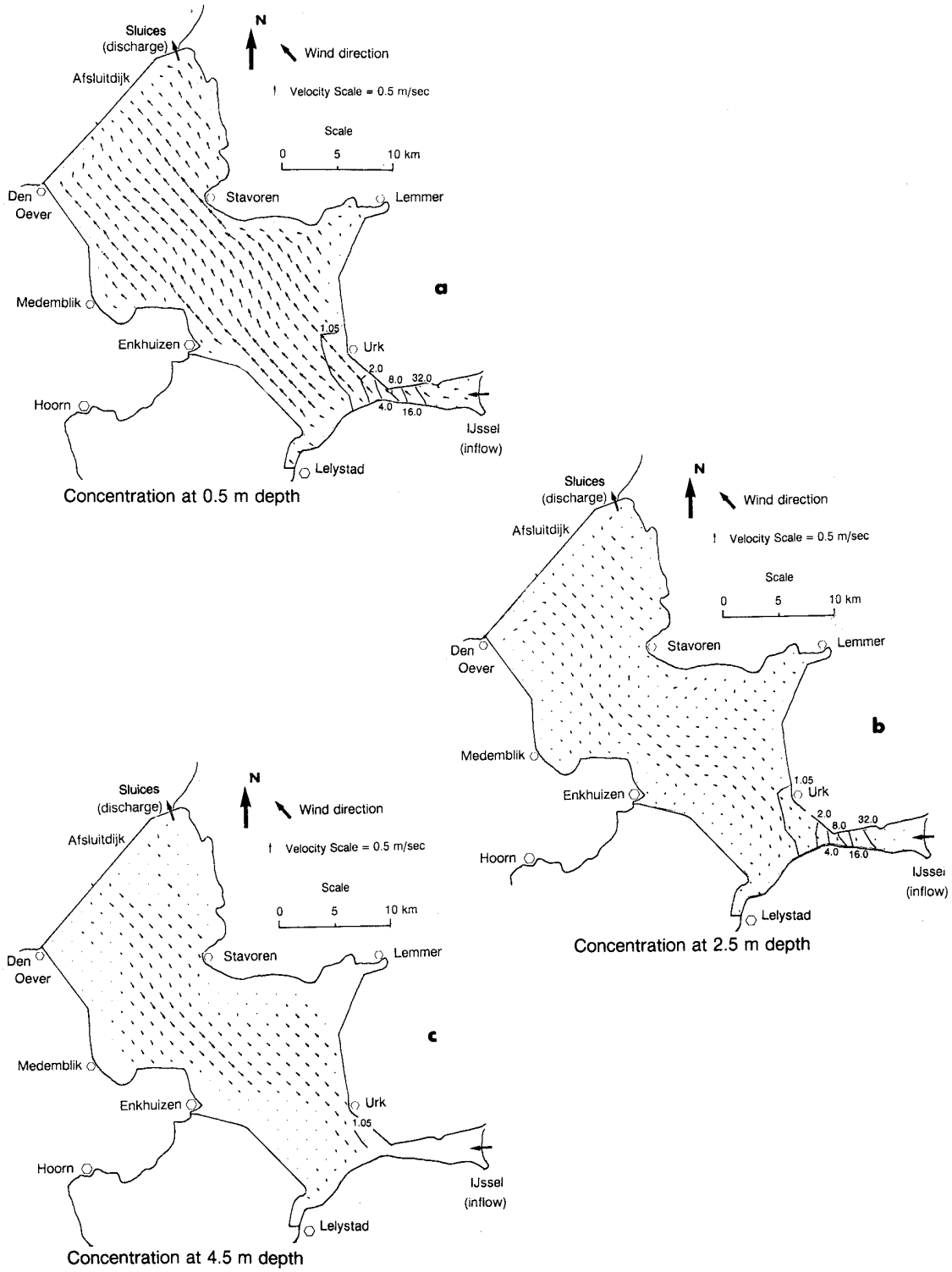

Fig. 8.4—Computed concentrations and velocities 24 hours after start of computation at 0.5 m depth (a), 2.5 m depth (b), and 4.5 m depth (c)

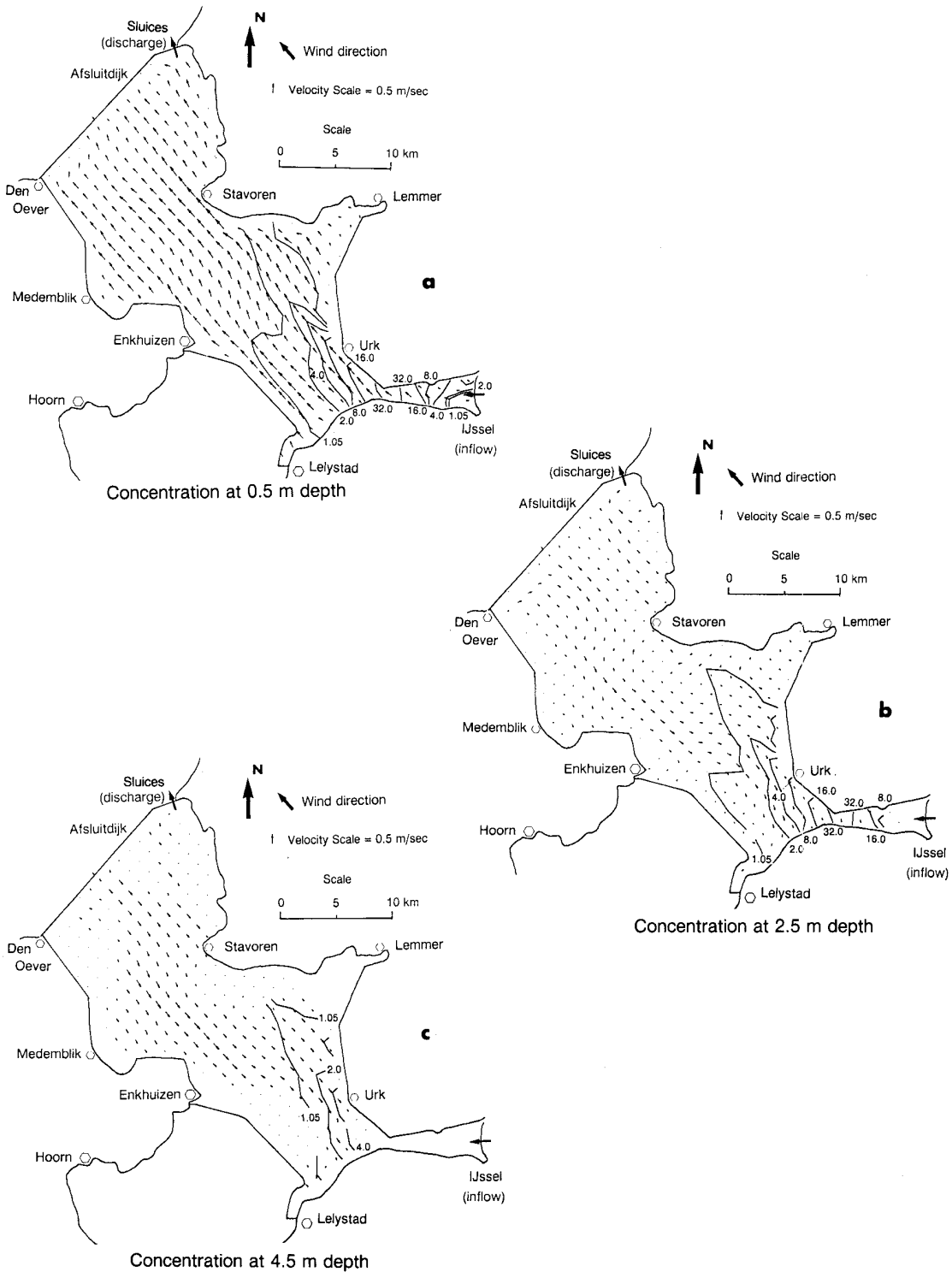

Fig. 8.5—Computed concentrations and velocities 48 hours after start of computation at 0.5 m depth (a), 2.5 m depth (b), and 4.5 m depth (c)

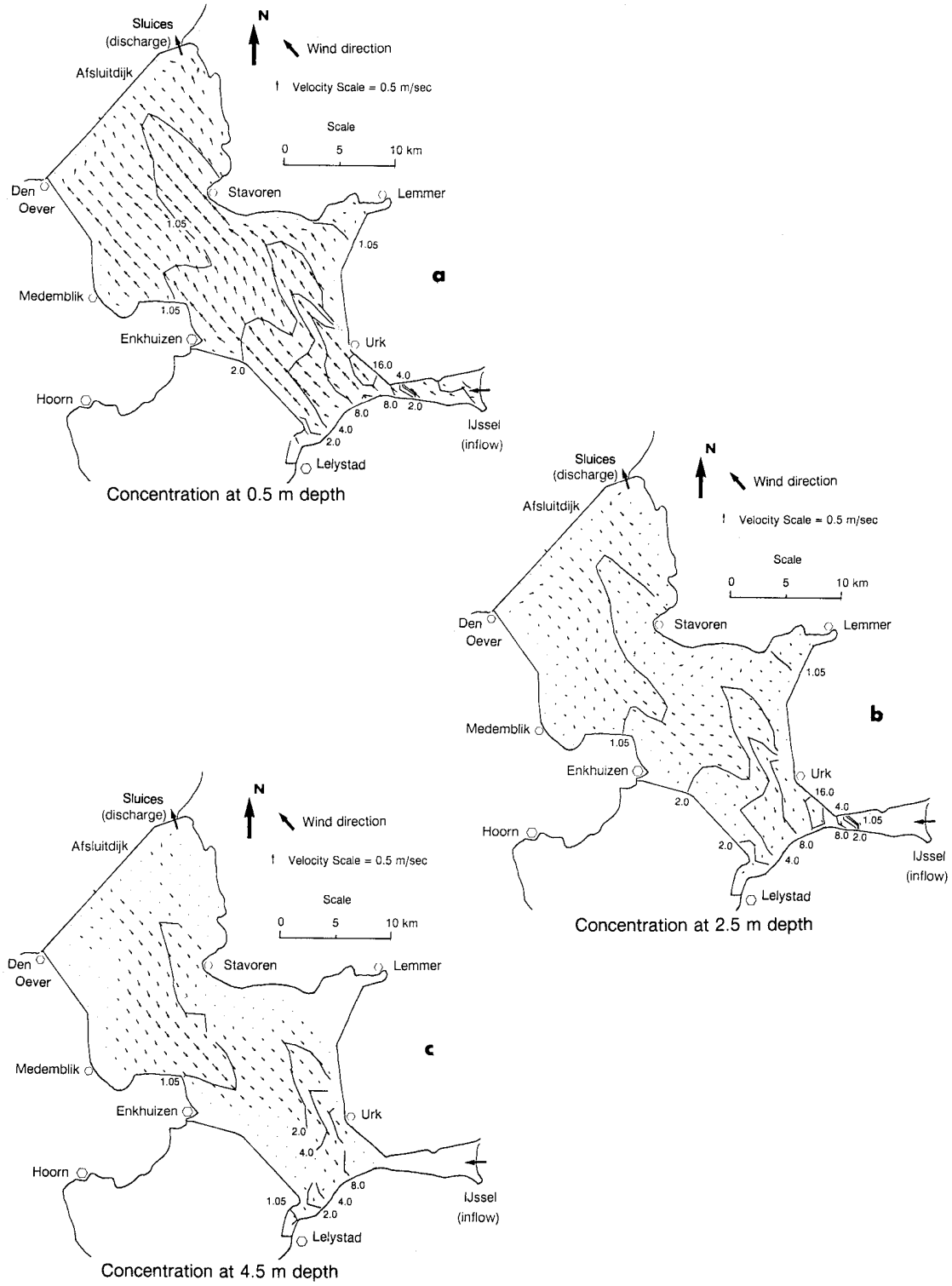

Fig. 8.6—Computed concentrations and velocities 72 hours after start of computation at 0.5 m depth (a), 2.5 m depth (b), and 4.5 m depth (c)

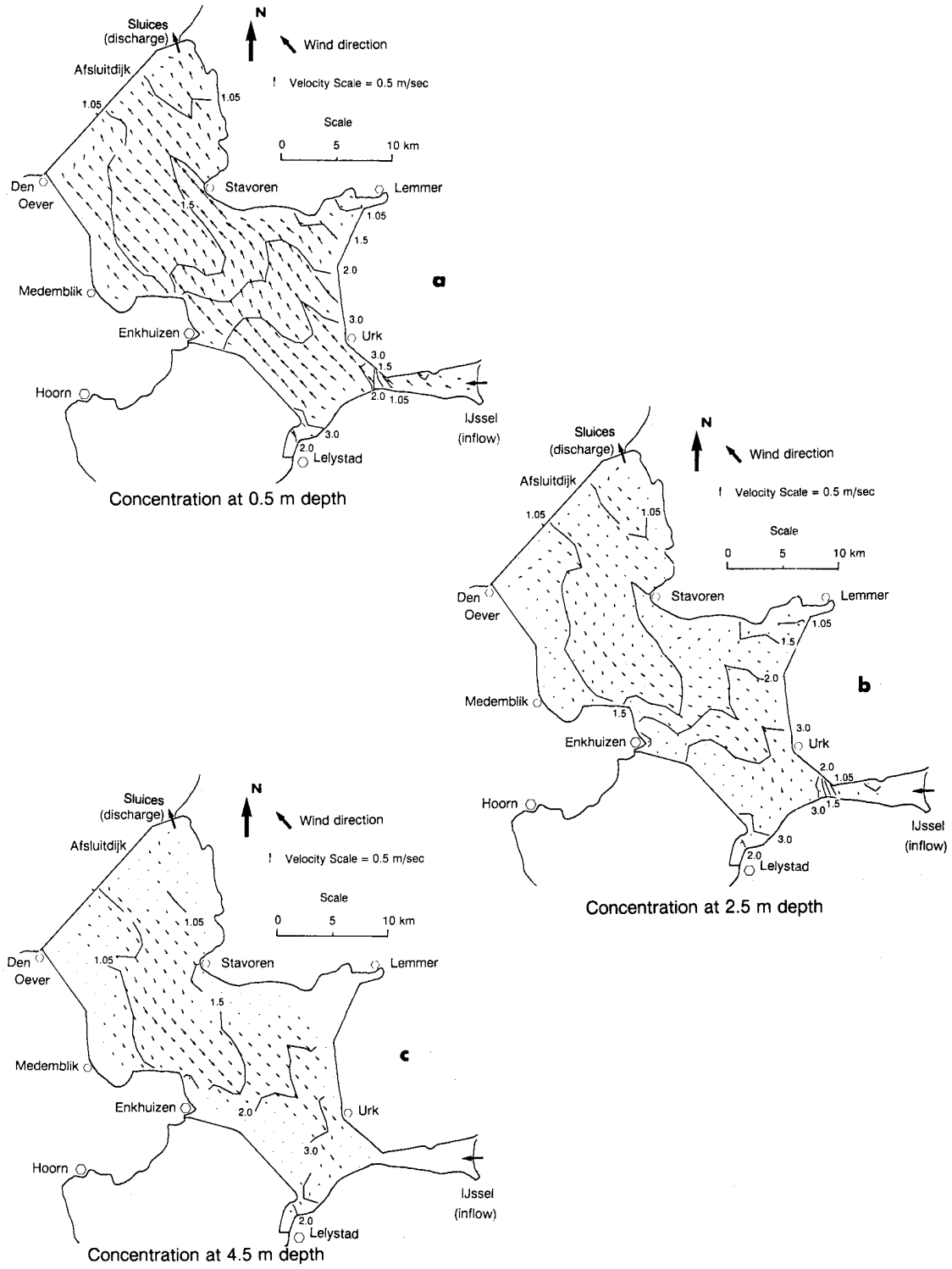

Fig. 8.7—Computed concentrations and velocities 96 hours after start of computation at 0.5 m depth (a), 2.5 m depth (b), and 4.5 m depth (c)

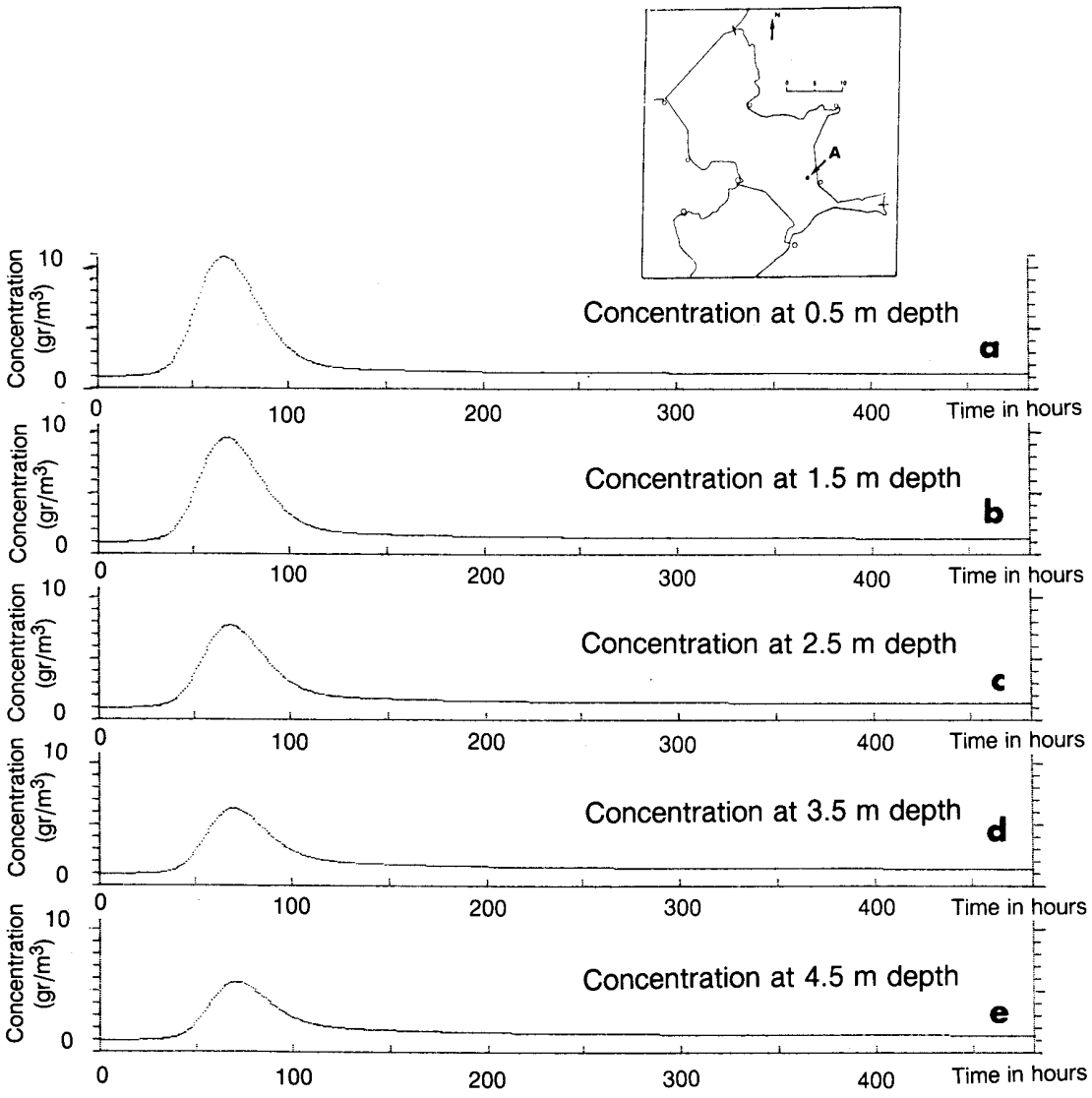

Fig. 8.8—Computed time series of the concentration at station A at 0.5 m depth (a), 1.5 m depth (b), 2.5 m depth (c), 3.5 m depth (d), and 4.5 m depth (e) (Δt = 7.5 min)

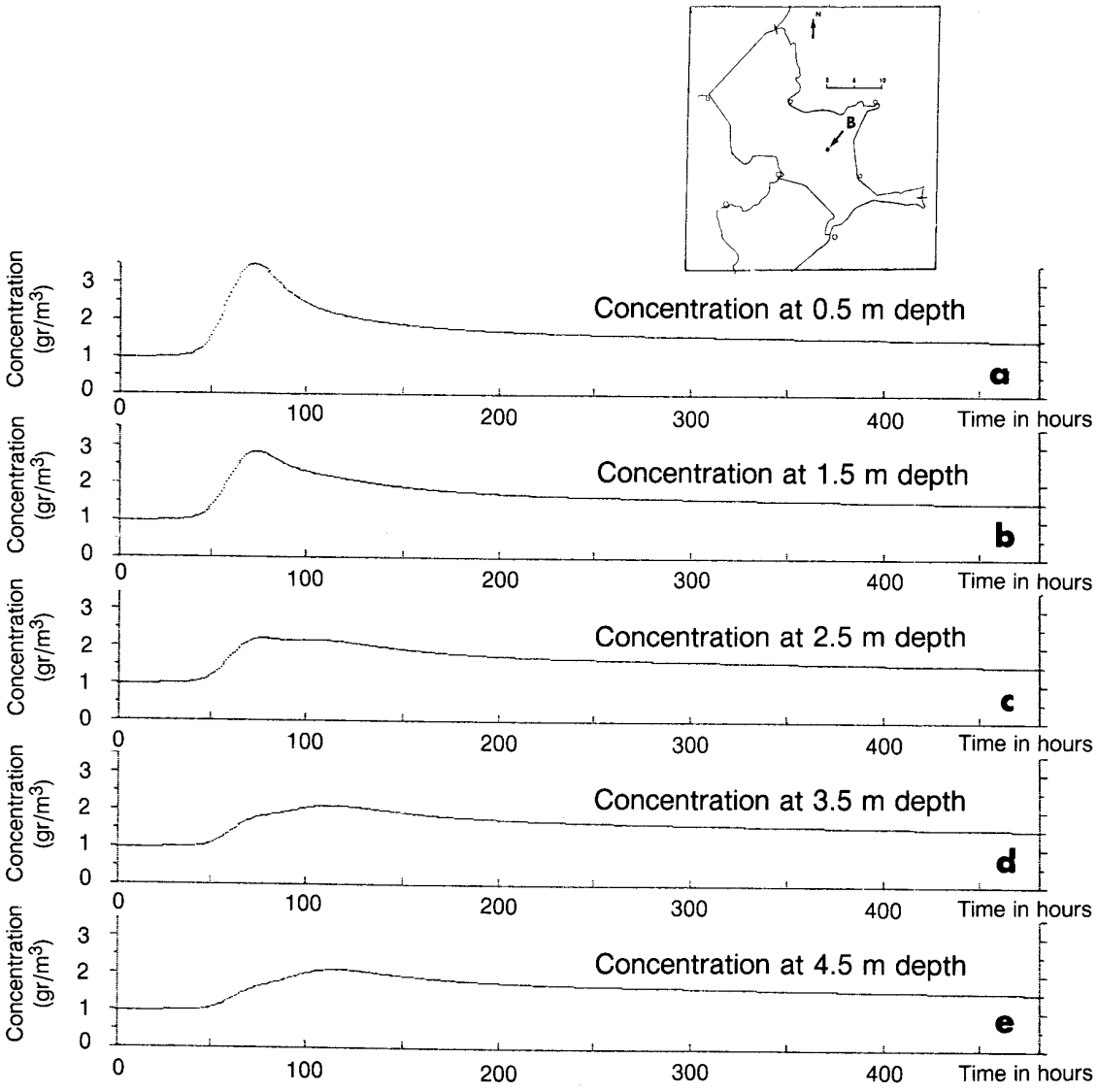

Fig. 8.9—Computed time series of the concentration at station B at 0.5 m depth (a), 1.5 m depth (b), 2.5 m depth (c), 3.5 m depth (d), and 4.5 m depth (e) (Δt = 7.5 min)

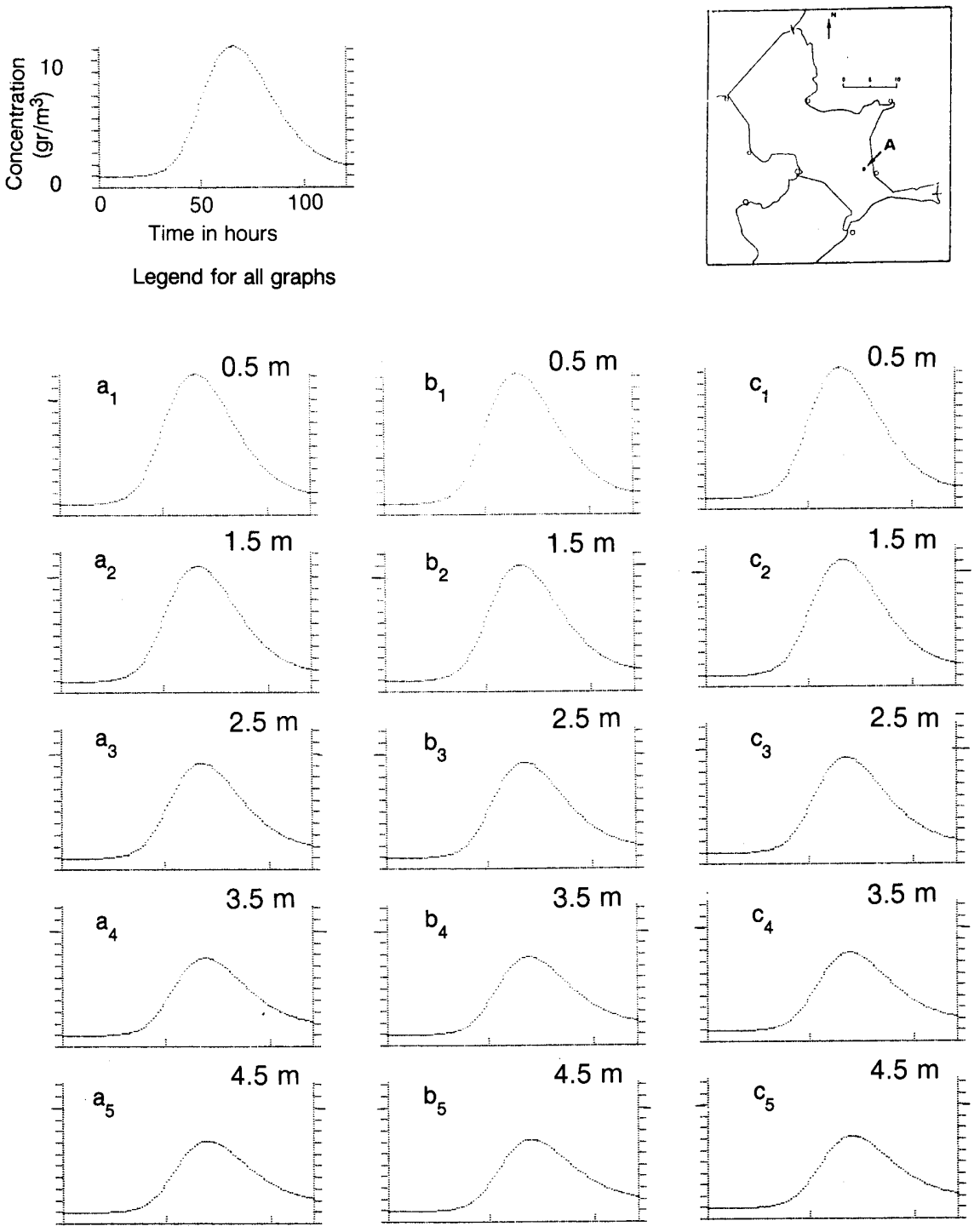

Fig. 8.10—Time series of the concentration at station A at different depth computed with a timestep of 5 min (a), 12 min (b), and 15 min (c)

momentum coefficients were taken to be very large. For both these coefficients, values of 0.1 m^2/sec were used. Such a high momentum exchange coefficient causes the velocities in any vertical to be essentially the same; thus the hydrodynamic computation is nearly the same as a two-dimensional vertically averaged model computation. The very high mass exchange coefficient causes very intense mixing in any vertical of the model; thus the computed concentrations are nearly the same as would be obtained with a vertically integrated two-dimensional model. Figure 8.11 shows the computed time series of the concentration at station B. The concentrations in all layers are essentially the same as was expected. In comparison with the three-dimensional model results (Fig. 8.9), it appears that the maximum concentrations are lower and that the arrival time is considerably delayed. Thus, it is very doubtful whether a two-dimensional model can give sufficient information for major policy decisions.

The last experiment with the lake model was an investigation of the behavior of a steep front. For the starting condition of the simulation, the northwestern part was given a concentration of a solute of 10 gr/m^3, whereas in the remainder of the lake the concentration was set to 1 grm^3, as shown in the insert of Fig. 8.12. The wind was again from the southeast with a speed of 11.3 m/sec. The horizontal momentum and mass exchange coefficients were set at 5 m^2/sec and the vertical exchange coefficients at 0.001 m^2/sec. Figure 8.12 shows the time series of the concentration at four stations "upwind" of the initial front. Because of the vertical circulation that is generated by the wind, water with a high concentration first reaches the station in the bottom layer. Note that the characteristic computational perturbations of the concentration before the arrival of the higher concentration are nearly completely absent. At stations at the other side of the initial front, shown in Fig. 8.13, we see also that the "overshoot" is very small.

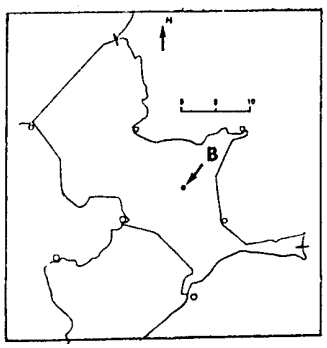

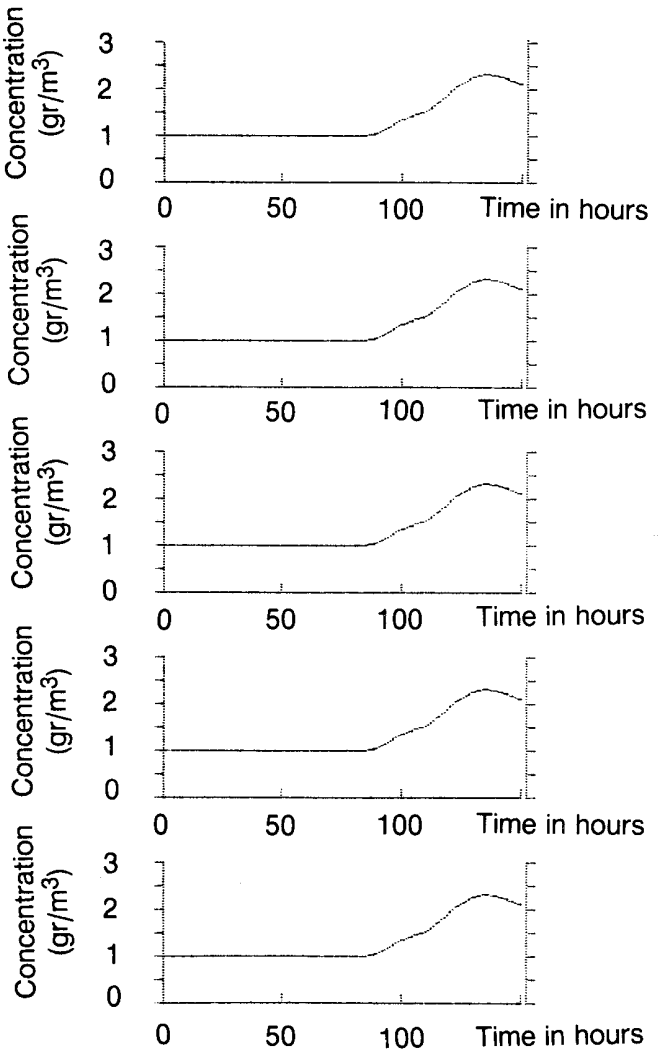

Concentration at 0.5 m depth

Concentration at 1.5 m depth

Concentration at 2.5 m depth

Concentration at 3.5 m depth

Concentration at 4.5 m depth

Fig. 8.11—Time series of the concentration at station B computed with vertical mass and momentum exchange coefficients valued at 0.1 m^2/sec at 0.5 m depth (a), 1.5 m depth (b), 2.5 m depth (c), 3.5 m depth (d), and 4.5 m depth (e) (Δt = 7.5 min)

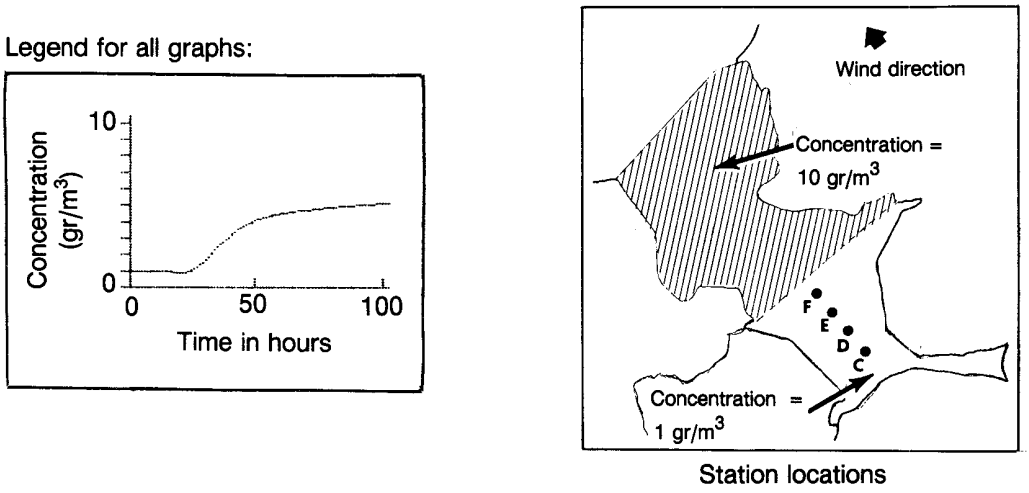

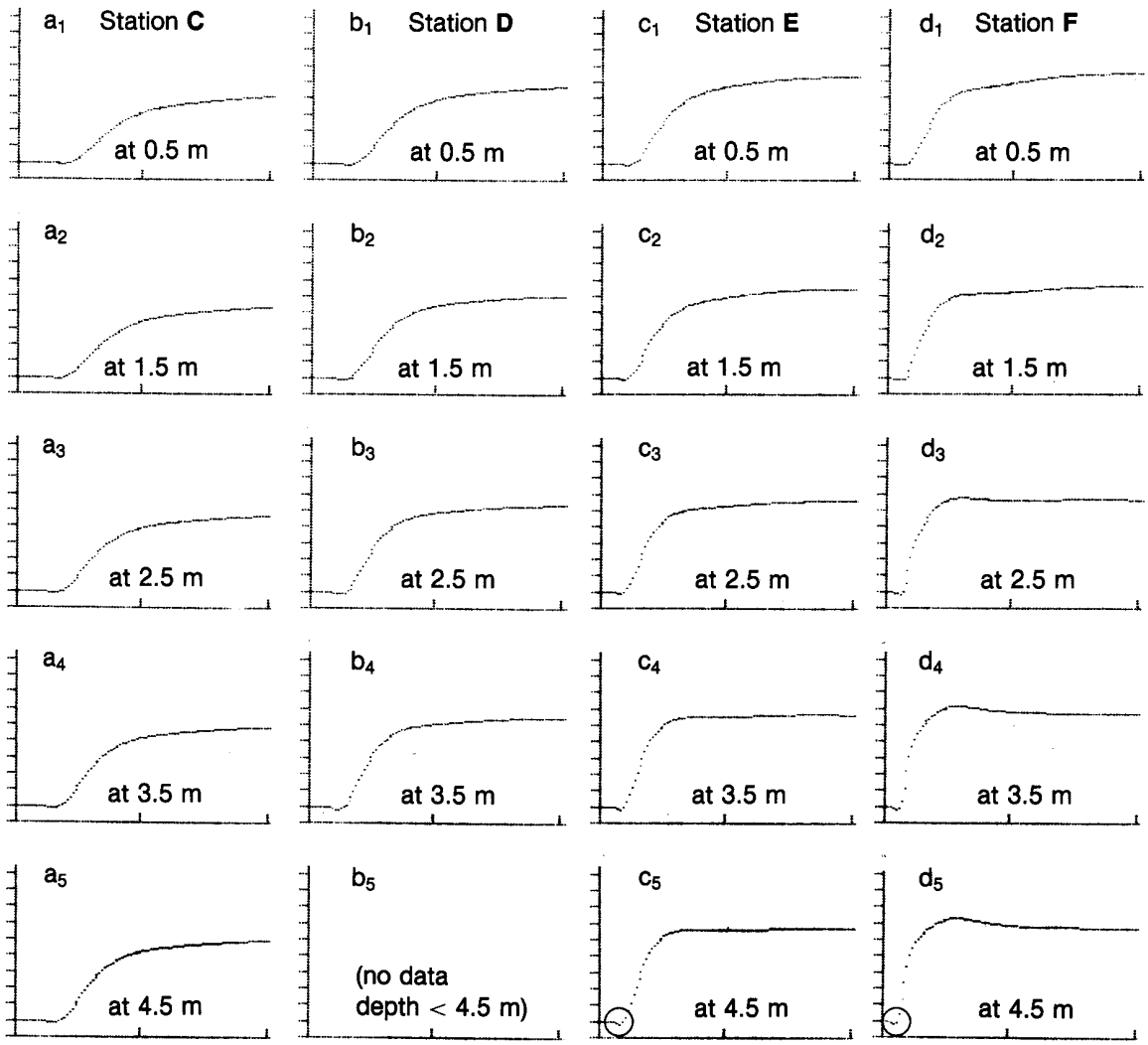

Fig. 8.12—Time series of the computed concentration at station C (a), D (b), E (c), and F (d) at different depth

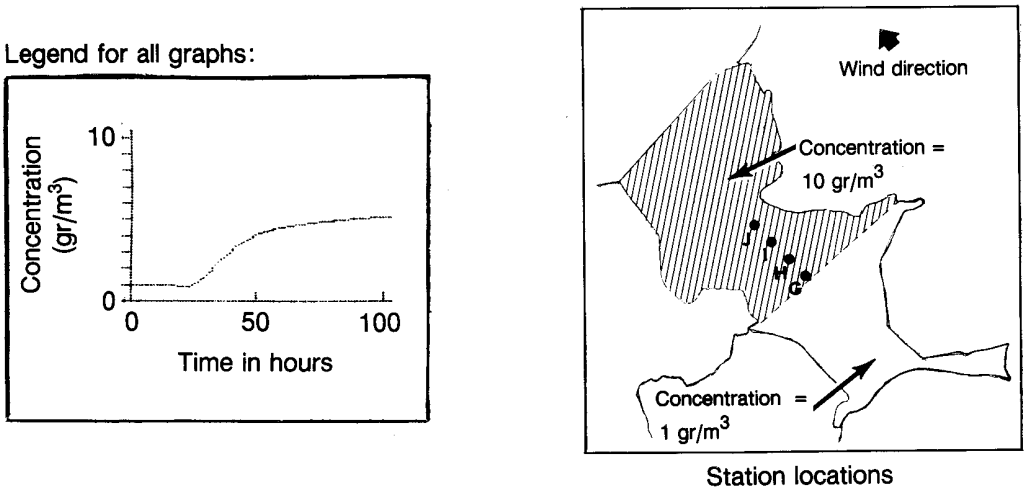

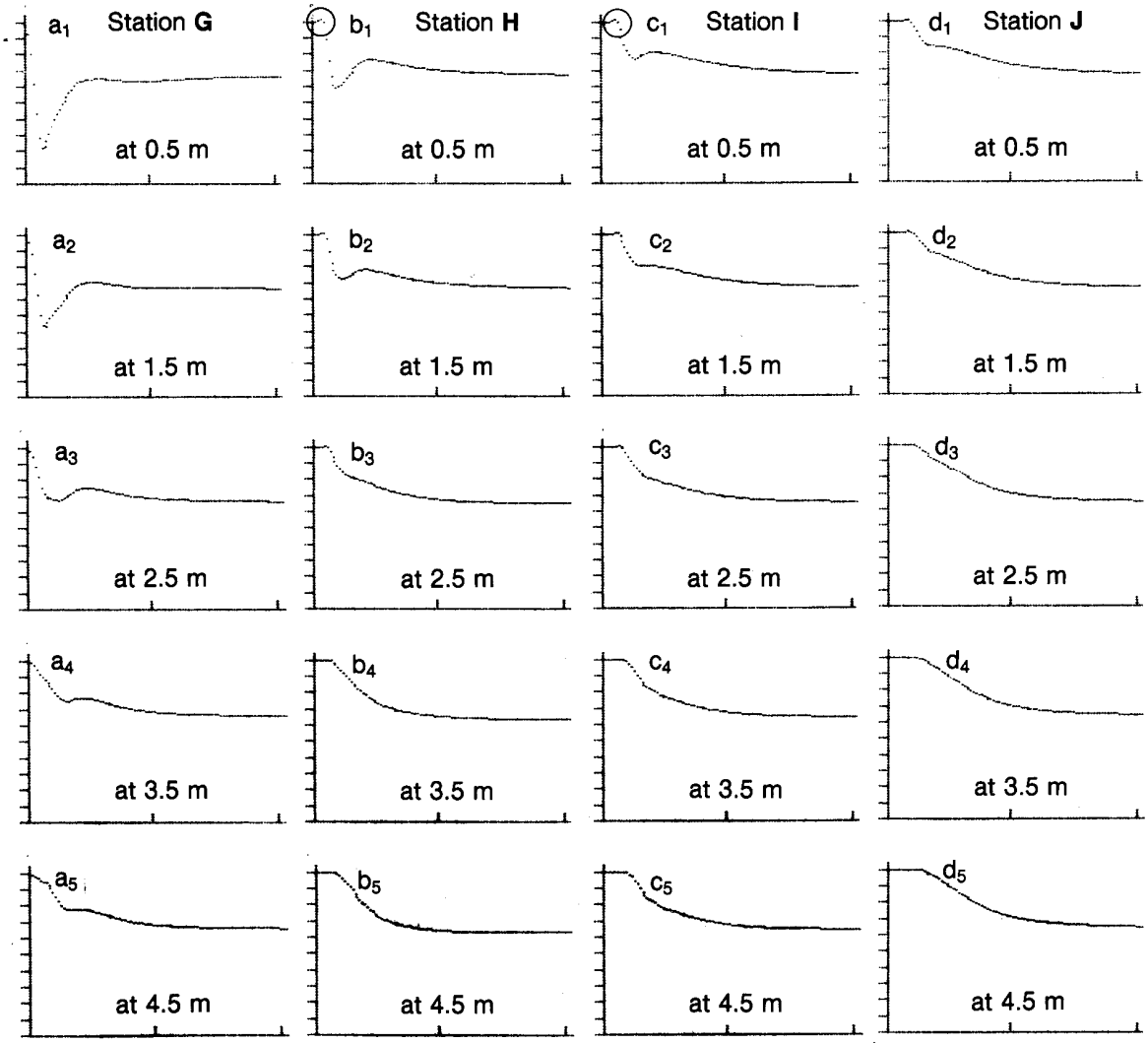

Fig. 8.13—Time series of the computed concentration at station G (a), H (b), I (c), and J (d) at different depth

IX. DISCUSSION

The main strength of the computation method appears to be the efficiency of the computation and the stability of the computation. The approximations of the finite difference equations are of a second order, and no filtering or the use of artificial viscosity is required for a stable computation with large timesteps. From the experiments in the rectangular basin, it is apparent that very short waves are not generated by the nonlinear terms. The choice of the advection terms is such that these introduce stability in the computation.

The general computation method that has been presented can be modified in many ways. For example, for the vertical advection and transport, central differences are still being used. These can be expressed also in the manner outlined in Sec. II, and the solution of matrices with variables in the vertical direction would then be replaced by explicit computation. Unfortunately, the boundary conditions then become more complex, and would require rather extensive experimentation.

The vertically integrated equations are solved by an alternating direction method. For each row or column in each direction, the vertical momentum equations are inserted in the vertically integrated continuity equation, and new sets of equations containing three unknown water levels are solved. It is possible also to use a completely implicit method for solving the water levels such as is used by Backhaus [14]. To modify the present algorithm would not be a major effort; the program part in which the vertically integrated equations are solved is small compared to the sections in which the velocities and concentrations are computed. It remains to be seen, however, if this would lead to a more efficient method for large models, as the computation time of the implicit method increases with a power function of the number of points in the two-dimensional water-level array.

From the experiments, it can be noted that a rectangular grid is used. The depth is approximated by discrete layers of a fixed thickness, except for the upper and bottom layer. This has very distinct advantages. The bottom can be represented quite accurately, without influencing the flow computations, as is the case when transformed vertical coordinates are being used. In practical application, when using vertical transformations with a strongly varying depth, the results are influenced considerably by the grid system. For example, when water flows from a tidal flat into an adjacent deep channel, the use of the transformed grid causes part of the water to be mixed into the bottom layer of the channel, which is very unrealistic, particularly when density differences are present. Moreover, much computation effort is wasted by computing in very shallow areas with much resolution in the vertical. The use of transformed vertical coordinates originates probably from a strong reduction in programming effort.

In this report, only flow without density differences was considered. Naturally density gradients resulting from temperature and salinity distributions in the water body need to be considered, and the model need only be extended for that purpose. A major part of that extension is already available in the transport model.

The experiments that were described in this report gave insight into the efficiency of the method. The first experiment indicates clearly that much larger timesteps are possible than with the earlier RAND model. The other example shows an application of the three-dimensional model of the type used for management studies. The simulations shown were all made on a personal computer (PC-AT). These applications show that with this new approach

to three-dimensional modeling, effective simulations for many problems can be made with engineering workstations.

X. CONCLUSIONS

The three-dimensional model based upon the finite difference approximations for the momentum equations, the continuity equations, and the transport equations described in this report allows very efficient modeling. The computation is stable, and the approximations are of a second order. The timestep of the computation is governed by the accuracy desired in the results.

Experiments show that simulations can be made with rather limited computation resources.

REFERENCES
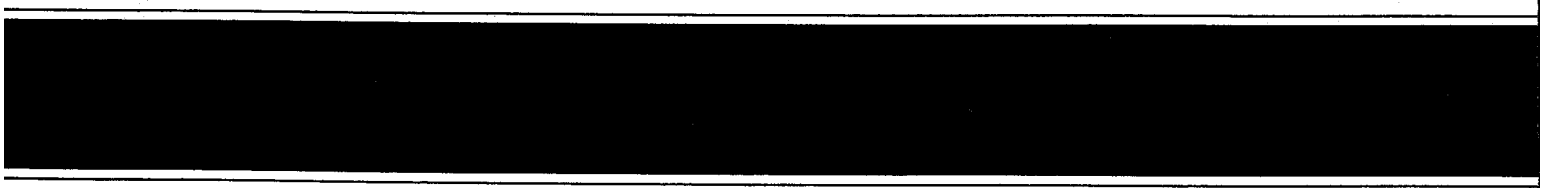
1. Leendertse, Jan J., Richard C. Alexander, and D.S.K. Liu, *A Three-Dimensional Model for Estuaries and Coastal Seas: Volume I, Principles of Computation*, The RAND Corporation, R-1417-OWRR, December 1973.
2. Leendertse, Jan J., and D.S.K. Liu, *A Three-Dimensional Model for Estuaries and Coastal Seas: Volume II, Aspects of Computation*, The RAND Corporation, R-1764-OWRT, June 1975.
3. Leendertse, Jan J., and Shiao-Kung Liu, *A Three-Dimensional Model for Estuaries and Coastal Seas: Volume IV, Turbulent Energy Computation*, The RAND Corporation, R-2187-OWRT, May 1977.
4. Liu, Shiao-Kung, and Alfred B. Nelson, *A Three-Dimensional Model for Estuaries and Coastal Seas: Volume V, Turbulent Energy Program*, The RAND Corporation, R-2188-OWRT, May 1977.
5. Liu, D.S.K., and Jan J. Leendertse, *A Three-Dimensional Model for Estuaries and Coastal Seas: Volume VI, Bristol Bay Simulations*, The RAND Corporation, R-2405-NOAA, September 1979.
6. Blumberg, A. F., and G. L. Mellor, *A Coastal Ocean Numerical Model*, Lecture Notes on Coastal and Estuarine Studies, in J. Sundermann and K. P. Holz (eds.), Springer-Verlag, 265 pp., 1980.
7. Blumberg, A. F., and G. L. Mellor, "Diagnostic and Prognostic Numerical Circulation Studies on the South Atlantic Bight," *J. Geophys., Res.*, Vol. 88, pp. 4579–4592, 1983.
8. Oey, Lie-Yauw, George L. Mellor, and Richard I. Hires, "A Three-Dimensional Simulation of the Hudson-Raritan Estuary. Part I: Description of the Model and Model Simulation," *Journal of Physical Oceanography*, Vol. 15, May 1985.
9. Sheng, Y. P., *Mathematical Modeling of Three-Dimensional Coastal Currents and Sediment Dispersion*, Technical Report CERC-83-2, U.S. Army Engineers Waterways Experiment Station, Vicksburg, MS.
10. Sheng, Y. P., S. F. Parker, and D. S. Hen, *A Three-Dimensional Estuarine Hydrodynamic Software (EHSM3D)*, Aeronautical Research Associates of Princeton, NJ.
11. Stelling, G. S., *On the Construction of Computational Methods for Shallow Water Flow Problems*, Thesis Delft, 1983. Also, Rijkswaterstaat Communications No. 35, Rijkswaterstaat, The Hague, The Netherlands, 1984.
12. Richtmyer, R. D., and K. W. Morton, *Difference Methods for Initial Value Problems*, Interscience Publishers, New York, 1957.
13. Leonard, B., "A Stable and Accurate Convective Modelling Procedure Based on Quadratic Upstream Interpolation," *Computer Methods in Applied Mechanics and Engineering*, Vol. 19, pp. 59–68, 1979.
14. Backhaus, Jan O., "On the Circulation of the Stratified North Sea," *Coastal Oceanography*, NATO Conference Series, Plenum, London, 1983.